Received: 17 October 2022 | Revised: 4 January 2023 | Accepted: 26 January 2023

DOI: 10.1002/jev2.12310

RESEARCH ARTICLE

Hypoxia promotes EV secretion by impairing lysosomal homeostasis in HNSCC through negative regulation of ATP6V1A by HIF-1α

Xiaoning Wang[1,2] | **Ruoyi Wu**[2] | **Peisong Zhai**[2] | **Zheqi Liu**[2] | **Ronghui Xia**[1] | **Zhen Zhang**[2] | **Xing Qin**[2] | **Chuwen Li**[2] | **Wantao Chen**[2,3] | **Jiang Li**[1] | **Jianjun Zhang**[2]

[1]Department of Oral Pathology, Shanghai Ninth People's Hospital, Shanghai Jiao Tong University School of Medicine, Shanghai, PR, China

[2]Department of Oral and Maxillofacial-Head and Neck Oncology, Ninth People's Hospital, School of Medicine, Shanghai Jiao Tong University, Shanghai, PR, China

[3]Shanghai Key Laboratory of Stomatology & Shanghai Research Institute of Stomatology, National Clinical Research Center of Stomatology, Shanghai, PR, China

Correspondence
Jianjun Zhang, Ninth People's Hospital, Shanghai Jiao Tong University School of Medicine, 639 Zhizaoju Road, Shanghai 200011, China.
Email: zjjbio@sjtu.edu.cn

Funding information
National Natural Science Foundation of China, Grant/Award Numbers: 82173148, 32000552, 81972573, 81872187, 82230090, 82141108; Innovative Research Team of High-level Local Universities in Shanghai under, Grant/Award Number: ZLCX20212301; Shanghai sailing program, Grant/Award Number: 20YF1424300; Shanghai Committee of Science and Technology, Grant/Award Number: 21DZ2292000

Abstract

Tumour cells under hypoxia tend to modulate the number and contents of extracellular vesicles (EVs) to regulate the tumour microenvironment (TME) and thus promote tumour progression. However, the mechanism of how hypoxia influences the secretion of EVs remains to be elucidated. Here, we confirm the increased production of EVs in head and neck squamous cell carcinoma (HNSCC) cells under hypoxia, where endosome-derived EVs are the main subtype affected by insufficient O_2. The accumulation of hypoxia-inducible factor-1α (HIF-1α) under hypoxia directly downregulates the expression of ATP6V1A, which is pivotal to maintain the homeostasis of lysosomes. Subsequently, impaired lysosomal degradation contributes to the reduced fusion of multivesicular bodies (MVBs) with lysosomes and enables the secretion of intraluminal vesicles (ILVs) as EVs. These findings establish a HIF-1α-regulated lysosomal dysfunction-EV release axis and provide an exquisite framework to better understand EV biogenesis.

KEYWORDS
ATP6V1A, extracellular vesicles, HIF-1α, hypoxia, lysosomes, multivesicular bodies

1 | INTRODUCTION

Small extracellular vesicles (EVs) are membrane-enclosed vesicles secreted into the extracellular environment by almost all cell types (van Niel et al., 2022). As major mediators of intercellular communication, EVs are involved in various physiological and pathological processes, which have attracted significant attention in recent years (Hou & Chen, 2021). According to the current knowledge, there are two different ways for the biogenesis of EVs: generation by the outward budding and fission of the plasma membrane and subsequent release into the extracellular space or originating in endosome compartments called multivesicular bodies (MVBs) (van Niel et al., 2018). Recently, the term 'ectosomes' was recommended to specifically refer to plasma-derived

Xiaoning Wang, Ruoyi Wu, and Peisong Zhai contributed equally to this work.

EVs, and 'exosomes' refer to MVB-derived EVs (Witwer & Thery, 2019). For details, exosomes originate in MVBs, which are late endosomes containing multiple intraluminal vesicles (ILVs) formed by the invagination of the endosomal membrane. MVBs are primarily destined to fuse with lysosomes, resulting in the degradation of their content. Alternatively, mechanisms intervening in their degradation will lead to the secretion of MVBs and subsequent release of exosomes (van Niel et al., 2022). Although regulation of the balance undoubtedly influences the biogenesis of exosomes, the underlying mechanism remains far from comprehensive.

The tumour microenvironment (TME), an internal physical and chemical condition in which cancer cells live, is recognized as a complicated milieu mostly characterized by hypoxia, low pH and nutrient deprivation (Hanahan & Weinberg, 2011). Hypoxia, referring to a reduction in tissue oxygen saturation, is one of the most comprehensively studied characteristics of the TME, and it is also a common feature in solid tumours (Jing et al., 2019). According to the study of Vinayak et al., head and neck squamous cell carcinoma (HNSCC) is one of the most hypoxic tumour of 19 tumour types based on the data in The Cancer Genome Atlas (TCGA) and the Canadian Prostate Cancer Genome Network (CPC-GENE) analysis (Bhandari et al., 2019). In recent decades, studies have revealed that tumour-derived EVs under hypoxia play an essential role in remodelling the TME and benefitting the progression (invasiveness, angiogenesis, proliferation, chemotherapy and radiation resistance, immune evasion, metabolism and cancer stemness, etc.) of several types of tumours, including HNSCC (Dorayappan et al., 2018; Guo et al., 2018; Hsu et al., 2017; Li et al., 2016; Patton et al., 2020; Ren et al., 2019; Rong et al., 2016; Shao et al., 2018). Undoubtedly, the increased production of EVs in response to hypoxia is significant to exert these functions; nevertheless, the underlying mechanism still needs further clarification.

As the main fate of MVBs is fusion with lysosomes, resulting in the degradation of their contents (van Niel et al., 2022), lysosomes are deemed to be the fate-determining point of MVBs, which means that the secretion of EVs has been associated with impaired lysosomal function. Lysosomes are acidic membrane-enclosed organelles responsible for the degradation of a variety of biomacromolecules in the endomembrane system and thus play a vital role in a multitude of cellular homeostatic pathways (Heaton et al., 2020; Saftig & Klumperman, 2009). The degradative function of lysosomes is carried out by over 60 luminal hydrolases whose catabolic reactions require the protected acidic environment of the lysosomes (Breiden & Sandhoff, 2019; Weber et al., 2020). However, confronted with various environmental stresses, organelles, including lysosomes, are prone to dysfunction (Xie et al., 2020). Research has showed that lysosome-associated membrane proteins (LAMPs) and cathepsin D (CTSD), a critical lysosomal protease, are downregulated in hypoxia-exposed trophoblasts, which eventually leads to lysosome dysfunction (Nakashima et al., 2020). Moreover, published data has consistently demonstrated that, in tumours, hypoxia and the subsequent acidosis induced by hypoxia could result in the movement of lysosomes to the cell periphery, the abnormal expression of LAMPs, an enlarged lysosomal compartment and the deacidification of the lysosomal lumen, all of which are related to impaired lysosomal activity (Damaghi et al., 2015; Glunde et al., 2003; Hong et al., 2019; Liu et al., 2018). Currently, the disorder of lysosomes in HNSCC and the underlying mechanisms were not fully understood.

Here, we present for the first time a detailed analysis of why the release of EVs is increased under hypoxia in HNSCC. We found that hypoxia impairs the function of lysosomes by reducing the expression of the constituent of V-ATPase on the surface of lysosomes, ATP6V1A. Following lysosome dysfunction, MVB fusion with lysosomes decreased, which finally promoted the secretion of EVs. Moreover, our study establishes that the expression of ATP6V1A is regulated by hypoxia-inducible factor-1α (HIF-1α).

2 | MATERIALS AND METHODS

2.1 | Patients and specimens

All the samples were collected from the Department of Oral and Maxillofacial-Head and Neck Oncolgy, Ninth People's Hospital, Shanghai Jiao Tong University School of Medicine (Shanghai, China). None of the patients in this study had previously received any radiotherapy or neoadjuvant chemotherapy, and the study was approved by the Ethics Boards of the Ninth People's Hospital. Additionally, the clinical stage was determined according to the 8th edition American Joint Committee on Cancer (AJCC) staging manual (Amin et al., 2017).

2.2 | Cell culture

CAL27 and SCC9 cells were purchased from the American Type Culture Collection (ATCC, USA), and HN6 were kindly provided by the University of Maryland Dental School, USA. CAL27 and HN6 were cultured in DMEM medium (BasalMedia, China) supplement with 10% foetal bovine serum (FBS; Gibco-BRL, USA), penicillin (100 units/mL) and streptomycin (100 μg/mL) at 37°C in a humidified 5% CO_2/95% air incubator, whereas SCC9 were maintained in DMEM/F-12 (BasalMedia, China) containing the same additives. Hypoxic treatment of cells was performed in a tri-gas incubator (ThermoFisher Scientific, USA)

flushed with a gas mixture of 1% O_2, 5% CO_2 and balanced N_2. Briefly, cells were seeded and cultured in normoxia for 12 h for attachment, and then transferred to hypoxic incubator to culture for a designated period of time.

2.3 | EV isolation

EVs were isolated based on the protocol described previously (Qin et al., 2019). Briefly, cells were cultured in medium containing Exosome-depleted FBS Media Supplement (SBI, USA). At 48 h after the preconditioning stimuli, the cell culture supernatant was collected and differentially centrifuged at 4°C for 10 min at 300 × *g*, then 15 min at 2000 × *g* and 45 min at 12,000 × *g* followed by filtration through a 0.22 μm PVDF filter (Millipore, USA). Finally, EVs were pelleted by ultracentrifugation at 120,000 × *g* for 70 min. The EVs were resolved in phosphate buffer saline (PBS) for the subsequent detection.

2.4 | Nanosight tracking analysis (NTA)

The size distribution and particle concentration were measured using a ZetaView particle tracker (ParticleMetrix, Germany) equipped with a 488 nm laser, at ×10 magnification, with Software Zetaview 8.05.02. For each measurement, three cycles were performed by scanning 11 cell positions each and capturing 30 frames per second. The measurement was done at 25°C and shutter of 70, then analysed by the following parameters: Maximum particle size: 1000, Minimum particle size: 5, Minimum particle brightness: 20.

2.5 | Transmission electron microscopy of EVs

For electron microscopy, the EV pellet was fixed with 2.5% glutaraldehyde in PBS buffer at pH7.4 overnight at 4°C. Then the samples were deposited on formvar/carbon-coated copper/palladium grids and absorbed for 10 min before uranyl/acetate negative staining for another 10 min. After air-drying the samples were observed under a transmission electron microscope (Hitachi-HT7800, Japan) at 80 kV.

2.6 | Western blotting

For western blotting analysis, EVs/cells were lysed with sodium dodecyl sulphate lysis buffer (SDS, Beyotime, China) and subjected to protein quantification using the BCA Protein Assay Kit (Thermo Fisher Scientific, USA). Then the protein samples were separated by 4%–20% polyacrylamide gels (Genshare biological, China) and transferred to 0.22-μm polyvinylidene fluoride (PVDF) membranes (Merck Millipore, USA). After blocked with 5% skimmed milk in PBS for 1 h at room temperature (RT), the blots were incubated with specific primary antibody overnight at 4°C. β-Actin was used as loading controls. Afterwards, the membranes were probed with HRP-conjugated secondary antibody (Beyotime, China) and visualized by Immobilon Forte Western HRP Substrate (Merck Millipore, USA) and Amersham Imager 600 system (General Electric Company, USA). The antibodies used in this study are listed in Table S1.

2.7 | Apoptosis analysis

5×10^5 cells were seeded in 6-well plates. After attachment, cells were cultured under normoxic or hypoxic condition for another 48 h. Then the cells were digested with trypsin (BD Biosciences, USA) and resuspended as single-cell suspension. Staining was performed according to the instructions of FITC Annexin V Apoptosis Detection Kit I (BD Biosciences, USA). Analysis was performed by flow cytometry(Beckman, CytoFLEX LX, USA)within 1 h. The data were analysed by FlowJo software.

2.8 | CCK-8 assay

Growth curve was carried out using CCK-8 assay. Briefly, cells were seeded into 96-well plates at a density of 1000 cells per well in five replicates. CCK-8 reagent (New Cell and Molecular Biotech, China) was diluted 10 times with culture medium and replaced the original medium. After incubated for 2 h at 37°C, the optical density (OD value) of each well was measured at 450 nm using a microplate reader (SpectraMax i3, Molecular Devices, USA).

2.9 | Lysosome isolation and immunoblot

After indicated treatment, the cells were collected with di. Lysosomes were then isolated from cells using the Lysosome Isolation Kit (Sigma-Aldrich, USA) on the basis of differential centrifugation followed by density gradient centrifugation method according to the manufacturer's protocol. Approximately 3×10^8 cells were subjected to lysosome isolation. The isolated lysosomes were resuspended in RIPA (Radioimmuno-precipitation assay) buffer supplemented with a protein inhibitor cocktail and phosphatase inhibitor to prevent protein degradation, blocking the activity of phosphatases, and were centrifuged at 16,000 × *g* for 30 min. The supernatant was transferred to a new 1.5 mL tube and subjected to protein quantification. Lysosome lysates (10 μg) were loaded onto 4%–20% polyacrylamide gels for subsequent immunoblotting.

2.10 | RNAseq and data analysis

The mRNA expression profiling was performed in cells exposed to 48-h normoxia and hypoxia using Illumina sequencing platform (oebiotech, Shanghai, China). Briefly, total RNA was extracted using Dynabeads﹨mRNA Purification Kit (Thermo Scientific, USA) and RNA integrity was evaluated using the Agilent 2100 Bioanalyser (Agilent Technologies, USA). The libraries were constructed using TruSeq Stranded mRNA LTSample Prep Kit (Illumina, USA) according to the manufacturer's instructions. Then these libraries were sequenced on the Illumina sequencing platform (HiSeqTM 2500 or Illumina HiSeq × Ten) and 125 bp/150 bp paired-end reads were generated. Pairwise significance analysis was performed using t-test with *P*-value cut-off of 0.01. The raw data are supplied in Supplementary File 1–2.

2.11 | Transmission electron microscopy of cells

Cells cultured on dishes were washed within PBS and fixed with 2.5% glutaraldehyde in 0.1 M phosphate buffer (PB, pH = 7.4) at room temperature (RT) for 2 h. Then, the cells were gently scraped and centrifugated for collection and rinsed three times with 0.1 M PB (15 min per wash). After pre-embedded with agarose, the cells were post-fixed with 1% OsO4 in 0.1 M PB for 2 h at 4°C. Then, samples that underwent the dehydration with gradient ethanol ranging from 30% to 100% (30%, 50%, 70%, 80%, and 90% for 20 min; 100% for 20 min two times), followed by acetone (two 15 min washes). After gradually embedded with two times of Spurr Kit (SPI, USA) and acetone (ratios of 1:1, 2:1 for 2 h at 37°C), samples were embedded in pure Spurr for 8 h at 37°C. Following, samples were inserted into the embedding models filled with pure Spurr and kept in 37°C oven overnight. Then the embedding models with resin and samples were moved into 65°C oven to polymerize for more than 48 h and finally sectioned using a Leica ultramicrotome (Leica Microsystems, Germany). Ultrathin sections (60–80 nm) were stained with 2% uranyl acetate saturated alcohol solution for 10 min in the dark, followed by lead citrate for 5 min avoiding CO_2. After rinsed with ultrapure water three times and dried overnight, the ultrathin sections were observed using a transmission electron microscope (HITACHI, Japan). The diameter of electron-dense lysosomes is determined by equivalent scale conversion in the enlarged image. For quantification of ILVs per MVB, ILVs and MVBs in more than 10 profiles of different cells were counted in a blind manner and only MVBs containing typical ILVs were counted.

2.12 | Immunofluorescence

For cell immunofluorescence assays, cells were cultured in confocal dishes with indicated treatment, and then fixed with 4% paraformaldehyde; for tissue immunofluorescence assays, frozen sections were fixed with cold acetone. After washed with PBS and penetrated with 0.5% Triton X-100, samples were blocked with 5% BSA and incubated with indicated primary antibodies (setting up blank group added no primary antibody) overnight at 4°C. Then samples were stained with Alexa Fluor 488-, Alexa Fluor 594- or Alexa Fluor 647-conjugated secondary antibodies (Abcam, USA; 1:200) for 1 h at RT. Cytoskeleton was visualized by FITC-phalloidin (Yeasen, China, 1:200) staining and nuclei was visualized by 4′,6-diamidino-2-phenylindole (DAPI; Yeasen, China, 1:5000) staining. Images were obtained with Nikon A1 scanning confocal microscope (Nikon, Japan). The diameter of LAMP1-positive lysosomes is determined by equivalent scale conversion in the enlarged image in high-power field (HPF). The ratio of co-localization is quantified by this basic rule: the number of RAB7-positive MVBs co-localized with LAMP1-positive lysosomes divided by the total number of LAMP1-positive lysosomes in one HPF.

2.13 | RNA extraction and real-time PCR analysis

Total RNA was extracted with TRIzol Reagent (Takara, Japan) according to the manufacturer's protocol and cDNA was synthesized using the PrimerScript RT reagent Kit (Takara, Japan). The real-time PCR reactions were performed using an ABI StepOne real-time PCR system (Life Technologies, USA) and the SYBR Premix Ex Taq reagent kit (Takara, Japan). The amplified PCR products were quantified and normalized using b-Actin as a control and all the PCR primers are provided in Table S2.

2.14 | LysoTracker assay

The lysosomal activity of the cells was measured using LysoTracker® Red DND-99 (Life Technologies, USA), which can accumulate in acidic compartments such as lysosomes due to proton trapping. For this experiment, LysoTracker media was made with a final concentration of 50 nM in normal cell culture media prior to staining and kept at 37°C in the dark until use. After removal of the original media at the end point of designated treatment, LysoTracker media was added, the cells were incubated for 20 min. Once the Lysotracker media was removed, cells were washed twice with PBS and fixed with 3% glutaraldehyde (Aladdin Biochemical Technology, China) in H_2O followed by nuclear staining with DAPI. Images were obtained with a Nikon A1 scanning confocal microscope. The number of Lysotracker$^+$ dots was determined by randomly selecting 3 areas for each sample using Image J software.

2.15 | LysoSensor assay

Measurement of lysosomal pH was performed using LysoSensor™ Yellow/Blue DND-160 (Invitrogen, USA). Cells were seeded onto a 96-well black microplate (1×10^4 per well). On the day of measurements, LysoSensor staining media was made with Hank's Balanced Salt Solution (HBSS) to a final concentration of 2 μM, which was preheated at 37°C in the dark until staining. After the cell media was removed and cells were washed with PBS, LysoSensor staining media was added (200 μL), and the cells were incubated for 25 min. Following the incubation, the media was removed, and the cells were washed twice with PBS and then left in 100 μL of fresh HBSS and fluorescence was measured quickly. All measurements were acquired with a SpectraMax i3x microplate reader with excitation at wavelength 329/395 nm and emission detection at 440/540 nm. Fluorescence1(F1) was measured with 329/440 nm and Fluorescence2(F2) was measured with 395/540 nm. X = 1 g(F2/F1), Y = lgpH, substitute F1 and F2 into the standard curve and calculate the pH value. Construction of the pH standard curve and calibrations of lysosomal pH followed a modification of a protocol described before (Ahmad & Leake, 2019; DePedro & Urayama, 2009; Heaton et al., 2020). Briefly, after staining with LysoSensor staining media, pH calibration buffer (pH 3.5, 4.5, 5.5, 6.5, 7.5, Bestbio, China) containing 20 μM Nigericin (MedChemExpress, USA) was added to the cells for 10 min. Then, measurements were acquired according to the method above, and one standard curve was required for each cell type.

2.16 | Lentiviral transduction and screening of stable strains

For gene silencing, the shRNA sequence of ATP6V1A was packaged into a PGMLV-Puro vector, and the sequences are provided in Table S3. Likewise, for gene overexpression, pcDNA3.1 lenti-PGK-Puro containing the human ATP6V1A or HIF-1α was synthesized. Then the vectors were packaged into lentivirus for subsequent transfection. The vector construction and lentivirus package were conducted by Shanghai Zorin Biological Technology Co., Ltd (China). HNSCC cells were transfected with lentiviral particles containing shATP6V1A, OE-ATP6V1A, OE-HIF-1α or respective empty vector. After 72 h of transfection, cells were treated with puromycin (Yeasen, China) at a final concentration of 5 mg/mL for 2 weeks to establish stable cell lines.

2.17 | Chromatin immunoprecipitation (ChIP)

ChIP assays were performed in HN6 and CAL27 cells subjected to hypoxia for 48 h with a ChIP Kit (Cell Signaling Technology, CST; USA) according to the manufacturer's instructions. Rabbit IgG was used as a control, and anti-HIF-1α antibody was used to pull down the promoter regions of ATP6V1A genes with the HIF-1α regulatory element. The DNA fragments were purified and used for real-time PCR with primers for the promoter of ATP6V1A. The results are presented as fold changes and were calculated by dividing the signals from ChIP obtained with the anti-HIF-1α antibody by those obtained with the IgG control. The primers used for this analysis are listed in Table S4.

2.18 | Luciferase reporter assay

After seeded onto 24-well plates for 24 h, the cells were transfected with 0.75 μg pGL3-basic-ATP6V1A promoter-luciferase reporter and 0.25 μg HIF-1α expression plasmid or empty vector along with 0.025 μg pRL-TK for normalization. Then the cells were cultured under hypoxia for 48 h until the luciferase activity was measured using the Dual Luciferase Reporter Assay System (Beyotime, China) according to the manufacturer's instructions.

2.19 | Reverse chromatin immunoprecipitation (reverse-ChIP)

A Reverse-ChIP kit (Bersin Bio, China) was used for this experiment. After culturing under hypoxia for 48 h, 3×10^8 cells were cross-linked with 3% formaldehyde for 10 min at RT, and then 0.125 M glycine was added to terminate the reaction. Cells were scraped to harvest, and chromatin DNA was sonicated to obtain ~500 bp fragments. The probes for ATP6V1A labelled with biotin were provided by Bersin Bio, and the sequences of the probes are listed in Table S5. The mixed probes at a final concentration of 1 nM per probe (predenatured at 85°C for 3 min) were added into the chromatin supernatant followed by a hybridization procedure (85°C for 10 min, 37°C for 30 min, 70°C for 5 min, 37°C for 30 min, 55°C for 2.5 min, 37°C for 60 min). Then, the supernatant was incubated for 2 h at 37°C with streptavidin magnetic beads. After rinsed for five times, elution buffer was added to resuspend the beads, and the protein was eluted by heating with shaking. Next, the protein samples were subjected to polyacrylamide gel electrophoresis, and the binding between the ATP6V1A promoter and transcription factors was verified by western blotting.

2.20 | Immunohistochemical analysis

For IHC, paraffin-embedded 3 μm thick sections were deparaffinized, rehydrated, submerged into citric acid buffer for heat-induced antigen retrieval, immersed in 0.3% hydrogen peroxide to block endogenous peroxidase activity, blocked with 3% goat serum albumin, and then incubated with primary antibodies at 4°C overnight and developed using the DAKO ChemMate Envision Kit/HRP (Dako-Cytomation, USA). Hematoxylin and dehydration were used to counterstain the nucleus. Then slides were submerged into graded ethanols and xylene and covered with coverslips. The histochemistry score was quantified using a semiautomated computerized image analysis system (Quant Center; Pannoramic MIDI/P250, 3DHISTECH, Hungary).

2.21 | Survival analysis based on TCGA datasets

Transcriptome data of TCGA HNSCC were downloaded from the Genomic Data Commons (GDC) portal via TCGA biolinks following a standard protocol (Mounir et al., 2019), and hypoxia score for each sample was calculated with the ssGSEA method from the R package Clusterprofiler based on the datasets with in the Gene Set Enrichment Analysis (GSEA database (http://www.gsea-msigdb.org/gsea/index.jsp). Kaplan-Meier analysis was performed to evaluate the prognosis potential of hypoxia score, and the results are shown as survival curves and the statistical significance was calculated by log-rank test.

2.22 | Statistical analysis

Statistical analyses in this study were conducted with SPSS19.0 software and Graphpad Prism 9.1. The data are presented as the mean $\pm$ standard deviation (S.D.) and all quantitative experiments were repeated with at least three independent biological repeats. The significance between two groups was analysed selectively by Student's *t*-test or Mann-Whitney *U* test for non-parametric tests, and significance among three or more groups was analysed by one-way ANOVA or Kruskal-Wallis test for non-parametric tests. A p-value < 0.05 (two-sided) was considered statistically significant.

3 | RESULTS

3.1 | Hypoxia promotes EV secretion

To analyse the role of hypoxia on the secretion of EVs, we first subjected the cells to hypoxia (1% O_2) for 48 h, and purified the secreted EVs from their conditioned media by a serial ultracentrifugation protocol as described previously (Qin et al., 2019).

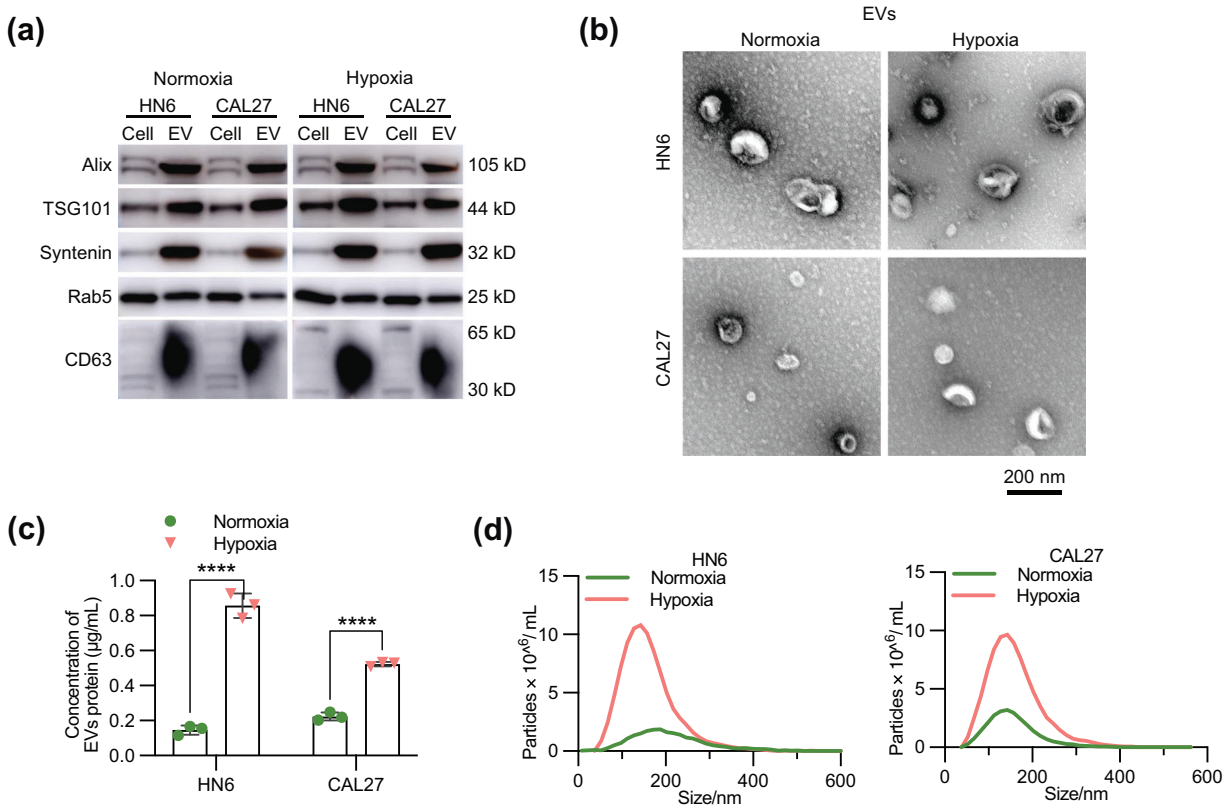

FIGURE 1 Hypoxia promotes EV secretion. (a) Western blot analysis of EVs purified by ultracentrifugation from cell CM from HN6 and CAL27 cells under normoxia or hypoxia for 48 h. Cells and EVs were blotted for the exosomal markers Alix, TSG101, Syntenin, Rab5 and CD63. (b) Representative electron microscopy images of EVs. Scale bar, 200 nm. (c) The EVs were collected from equal numbers of cells and concentration of EV protein was measured using BCA assay. (d) The size and quantity of normoxic and hypoxic EVs were measured using NTA. EVs were collected from 20×10^6 cells for each group. Statistical analyses were performed using *t*-test. ****P-value < 0.0001. Data are presented as the mean ± S.D.

Western blot analysis confirmed EV markers Alix, TSG101, syntenin, Rab5 and CD63 for both normoxic and hypoxic EVs (Figure 1a). In addition, transmission electron microscopy (Mounir et al.) validated that the EVs were approximately 100 nm in diameter and exhibited a typical cup-shaped morphology (Figure 1b). The measurement of EV protein levels and nanoparticle tracking analysis (NTA) showed an increased in EV secretion under hypoxia (Figure 1c,d). Besides, to exclude that EV release changes were associated to cell death, after cells were exposed to hypoxia for 48 h, the rate of apoptosis was measured by flow cytometry. There was no significant difference between two groups (Figure S1a). Moreover, the proliferation of cells under normoxic or hypoxic condition was evaluated using CCK-8 assays. Likewise, no obvious difference was observed within 72 h (Figure S1b).

3.2 | Hypoxia increases the secretion of endosome-derived EVs by inhibiting the fusion of MVBs with lysosomes

It is generally accepted that EVs are a heterogeneous group comprising exosomes and ectosomes, which originate from the endosomal system or form by direct outward budding from the plasma membrane, respectively. Although there is a lack of recognized protein markers to distinguish exosomes from ectosomes so far, some reliable studies have provided evidence to identify several markers that could be used as exosome or ectosome-specific markers (Mathieu et al., 2021). To determine which way of EV biogenesis is more affected by hypoxia, we analysed the expression of published markers indicating endosome- or budding-derived EVs. The data suggested that the number of EVs originating from the endosomal system increased when exposed to hypoxia, while the number of EVs generated by outward budding were decreased to some extent (Figure 2a). As the endosomal sorting complexes required for transport (ESCRT) pathway is essential for the formation of MVBs and the secretion of MVB-derived EVs, we examined the effect of hypoxic conditions on the levels of typical ESCRT components in HNSCC cells using an mRNA microarray and found that hypoxic cells exhibited a significant increase in the levels of most subunits of the ESCRT-I, II, III and Vps4 complex, but not ESCRT-0 (Henne et al., 2011), compared with normoxic cells (Figure 2b). This result suggested a more

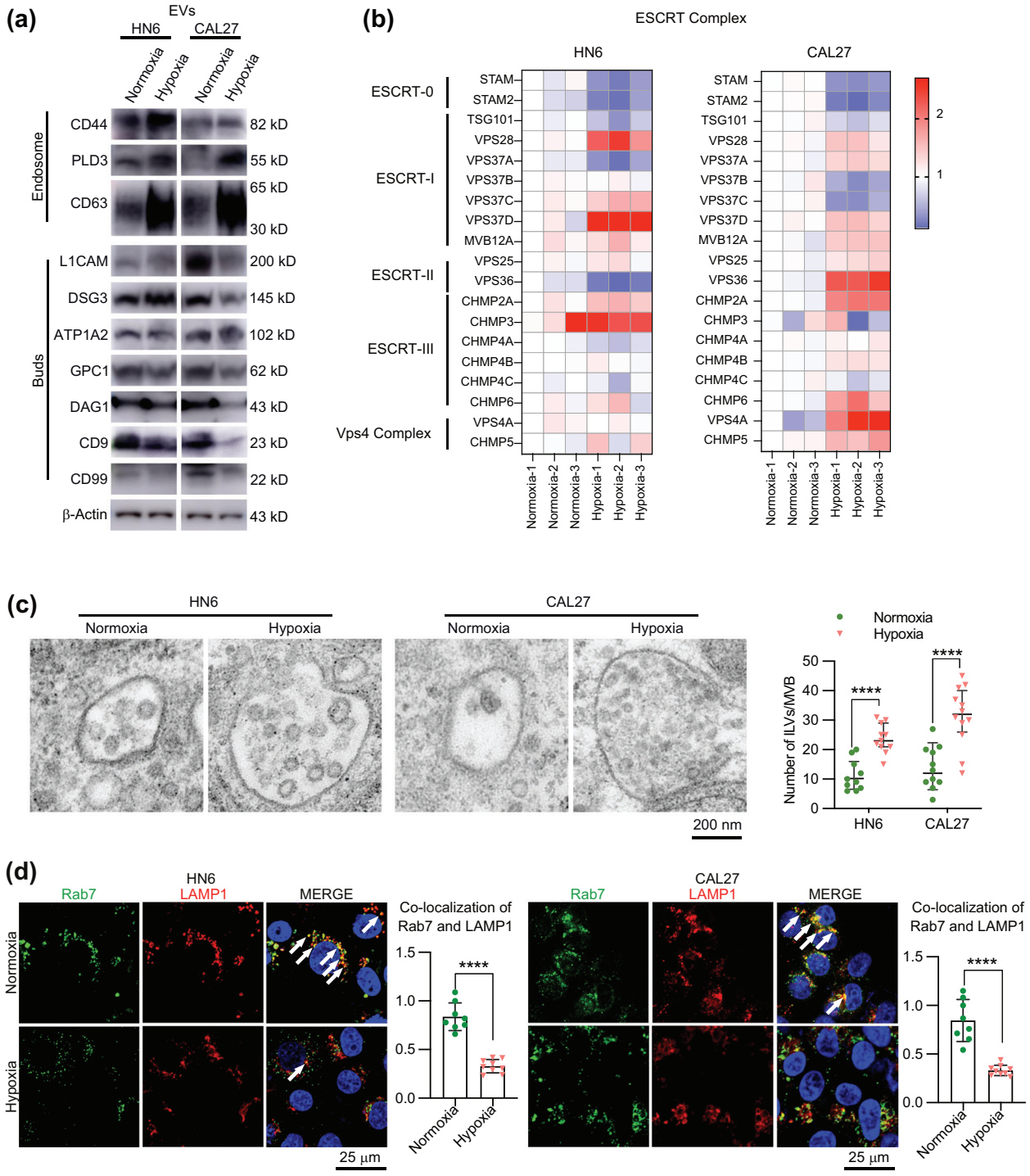

FIGURE 2 Hypoxia increased the secretion of endosome-derived EVs. (a) Representative western blot of normoxic and hypoxic EVs, using β-Actin as loading control. (b) The heatmap showed the different mRNA levels of ESCRT components in cells under normoxia and hypoxia for 48 h. (c) Representative electron microscopy images of MVBs in normoxic and hypoxic cells. Right graph: quantification of ILV number per MVB. Each dot represents the number of ILVs per MVB ($n > 10$ per group). Scale bar, 200 nm. (d) Confocal co-localization analysis of lysosomal maker LAMP1 and MVB marker Rab7 (green) in HN6 and CAL27 cells exposed to normoxia or hypoxia for 48 h. Scale bar, 25 μm. The ratio of co-localization of LAMP1 and Rab7 was quantified ($n > 10$ per group). Statistical analyses were performed using t-test. ****P-value < 0.0001. Data are presented as the mean $\pm$ S.D.

active endosomal system in hypoxia. Furthermore, we observed an alteration in MVB morphology using TEM, as the images showed an increased number of ILVs in MVBs when cells were under hypoxia (Figure 2c). However, TEM did not reveal any significant change in MVB density.

In the endosomal transport network, Rab5 is located in early endosomes and regulates the formation and fusion of early endosomes, whereas Rab5-Rab7 conversion represents the transition from early to late endosomes, also known as the maturation

of MVBs (Baietti et al., 2012; Galvez et al., 2012; Stenmark, 2009). We preliminarily examined the expression of Rab5 and Rab7 in response to oxygen insufficiency, and the data showed no clear difference (Figure S2a,b). Then, we detected the co-localization of Rab7 with LAMP1, a well-known marker of lysosomes, and found that hypoxia could prevent the fusion of MVBs with lysosomes (Figure 2d). Taken together, these results indicate that hypoxia mainly increases the secretion of EVs of endosomal origin, and this effect might contribute to the disruption of the lysosomal degradation of MVBs in HNSCC cells.

3.3 | Hypoxia impairs lysosomal function by destroying acidification of the lysosomal lumen

Next, to determine whether the deficiency of lysosomal function could influence the biogenesis of EVs, we treated tumour cells with the v-ATPase inhibitor bafilomycin A1 (Baf A1), which can lead to clear lysosomal alkalinization (Figure S3a), and then detected the release of EVs. NTA confirmed an increase in EV secretion after 24 h of treatment with Baf A1 (Figure 3a). Subsequently, we assessed the effect of hypoxia on the expression of LAMPs and two typical cathepsins in the lysosomal lumen (CTSB and CTSD) (Yang & Wang, 2021), and found no significant change at either the mRNA or protein level (Figure 3b,c). As enlarged compartment and redistribution are reported to be signs of lysosomal impairment (Fernandez-Mosquera et al., 2019; Walton et al., 2018), an immunofluorescence assay was used to evaluate the change in lysosome size and location. The data showed that the lysosome volumes were notably enlarged under hypoxic conditions, while the number of LAMP1-positive compartments was not affected (Figure 3d). Besides, we noticed that lysosomes tended to peripherally disperse throughout the cell in hypoxia (Figure S3b). Because lysosomes have a specific morphological signature with electron-dense contents that are easily recognized by electron microscopy, TEM images were acquired and further confirmed the same results (Figure 3e). We also performed immunofluorescence staining to detect the morphology of the lysosomes in HNSCC samples, and notably, the lysosomes in tumour cells were much larger than those in normal epithelial cells (Figure S4). LysoTracker probes are fluorescent acidotropic probes for labelling and tracking acidic organelles in live cells, which were used here to investigate the acidification of lysosomes in this study. Normoxic and hypoxic cells were incubated with the probes, and fluorescence intensity analysis suggested that the acidic environment in the lysosomal lumen was destroyed (Figure 3f). Furthermore, a LysoSensor assay was performed to assess the pH of the lysosomes, and an increased lysosomal pH value was observed after the cells were exposed to hypoxia (Figure 3g). Collectively, these results demonstrated that hypoxia could lead to an imbalance in the acidic environment in the lysosomal lumen rather than disrupt their biogenesis. Moreover, as a solid tumour prone to hypoxia, HNSCC cells are undoubtedly confronted with lysosomal impairment.

3.4 | ATP6V1A is required for basal lysosomal function

The acidic lysosomal lumen is maintained by the lysosomal v-ATPase, a large multisubunit complex composed of different proteins that are organized into a water-soluble, ATP-hydrolysing V1 domain and a membrane-embedded V0 proton channel, which function together by coupling the energy of ATP hydrolysis to the transport of protons across the lipid bilayer of the lysosomes (Forgac, 2007; Oot et al., 2017). To confirm which subunit isoform is mainly influenced by hypoxia, we investigated the expression of all subunits forming the complex and found that the expression of ATP6V1A was significantly repressed under hypoxia (Figure 4a and Figure S5a). Subsequently, the immunoblotting analysis showed that ATP6V1A protein was notably downregulated both in the whole-cell lysate and the lysosomal lysate (Figure 4b).

To evaluate the effects of ATP6V1A on lysosome homeostasis, we prepared a cellular model with stable shRNA-mediated knockdown of ATP6V1A in HN6 and CAL27 cells, and shRNAs with scramble sequences were used as controls (Figure S5b). Then, LysoTracker and LysoSensor assays were performed to assess the acidification and pH value of the lysosomes in shNC/shATP6V1A cells. The results indicated a neutral lysosomal environment after the downregulation of ATP6V1A (Figure 4c,d). Moreover, the size of the LAMP1-positive puncta obviously increased in shATP6V1A cells (Figure 4e), and similarly, the reduced level of LAMP1 and RAB7 colocalization indicated a less fusion of lysosomes with MVBs (Figure 4f). Next, to determine the influences of ATP6V1A on the biogenesis of EVs, we first investigated the morphology of MVBs. Unsurprisingly, the density of ILVs inside the MVB was higher in shATP6V1A cells than in control cells (Figure 4g). Finally, an increased level of EV release was confirmed when ATP6V1A was repressed (Figure 4h,i).

To verify the functions of ATP6V1A under hypoxic conditions, we constructed stable ATP6V1A-overexpressing cell lines using lentivirus (Figure S5c) and carried out a series of rescue experiments. The data clearly revealed that the exogenous expression of ATP6V1A could increase the LysoTracker dye intensity (Figure 5a), reinstate acidification of the lysosomal lumen impaired by hypoxia (Figure 5b), and restore the lysosomes to normal volume (Figure 5c). Undoubtedly, the co-localization of LAMP1 and Rab7 was reduced (Figure 5d), and the average number of ILVs per MVB was decreased by the overexpression of ATP6V1A (Figure 5e). More importantly, ATP6V1A recovery effectively repressed the secretion of EVs under hypoxia (Figure 5f,g). However, the overexpression of ATP6V1A did not have a significant impact on lysosomal homeostasis in normoxia (Figure S6). All

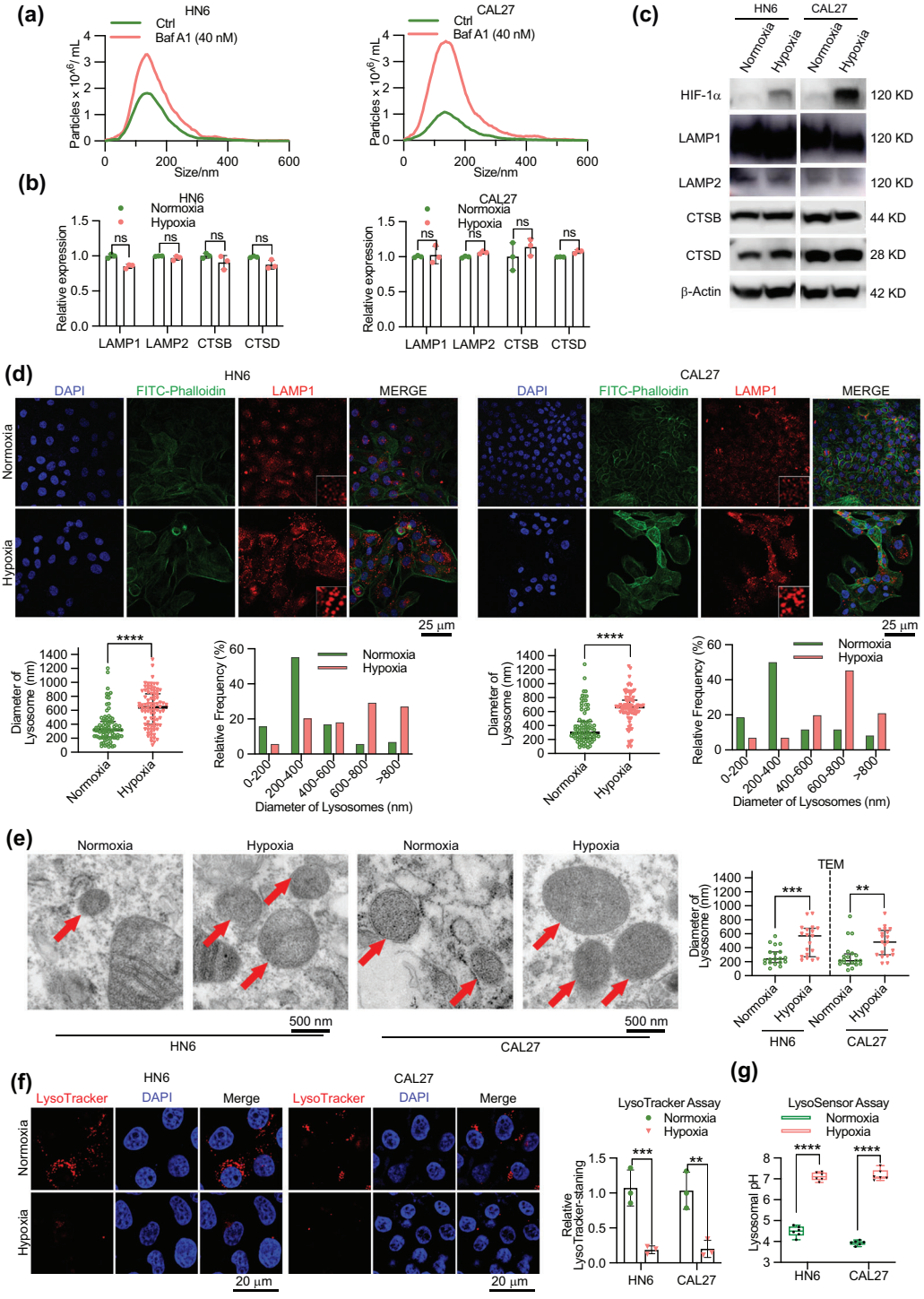

FIGURE 3 Hypoxia impairs the lysosomes. (a) NTA analysis of EV secretion in HN6 and CAL27 cells treated with DMSO (Ctrl) or DMSO with Bafilomycin A1 (Baf A1) for 24 h. (b) Real-time PCR was used to detect the effect of hypoxia on the expression of LAMP1, LAMP2, CTSB and CTSD. (c) Western blot was used to assess the protein level of LAMP1, LAMP2, CTSB and CTSD in HN6 and CAL27 cells exposed to normoxia or hypoxia for 48 h. (d) Confocal microscopy analysis of the lysosome marker LAMP1 in HNSCC cells exposed to normoxia or hypoxia for 48 h. Nuclei were stained with DAPI and cytoskeletons were stained with FITC-Phalloidin. Scale bar, 25 μm. The box plot on the lower left panel shows the distribution of the lysosomal diameter obtained for each condition, obtained from three independent experiments ($n > 80$ per group). The histogram on the lower right panel indicates the frequency distribution of lysosomal diameter in the normoxic and hypoxic cells, showing that the hypoxic cells have less small lysosomes (diameter < 400 nm) and a robust increase in the amount of very large lysosomes (diameter > 800 nm). (e) Representative electron micrographs showing electron-dense lysosomes (red arrows) in normoxic or hypoxic cells. Scale bar, 500 nm. Right graph: distribution of the lysosomal size across at least 10 cells obtained for each condition ($n > 20$ per group). (f) HNSCC cells were exposed to normoxia or hypoxia for 48 h and then stained with Lysotracker Red. Scale bar, 20 μm. The number of Lysotracker$^+$ dots was quantified. (g) Lysosomal pH was determined using Lysosensor™ Yellow/Blue DND-160. Each dot represents a lysosomal pH value in an independent experiment. Statistical analyses were performed using *t*-test. ns, no significance, ** *P*-value < 0.01, *** *P*-value < 0.001, **** *P*-value < 0.0001. Data are presented as the mean ± S.D.

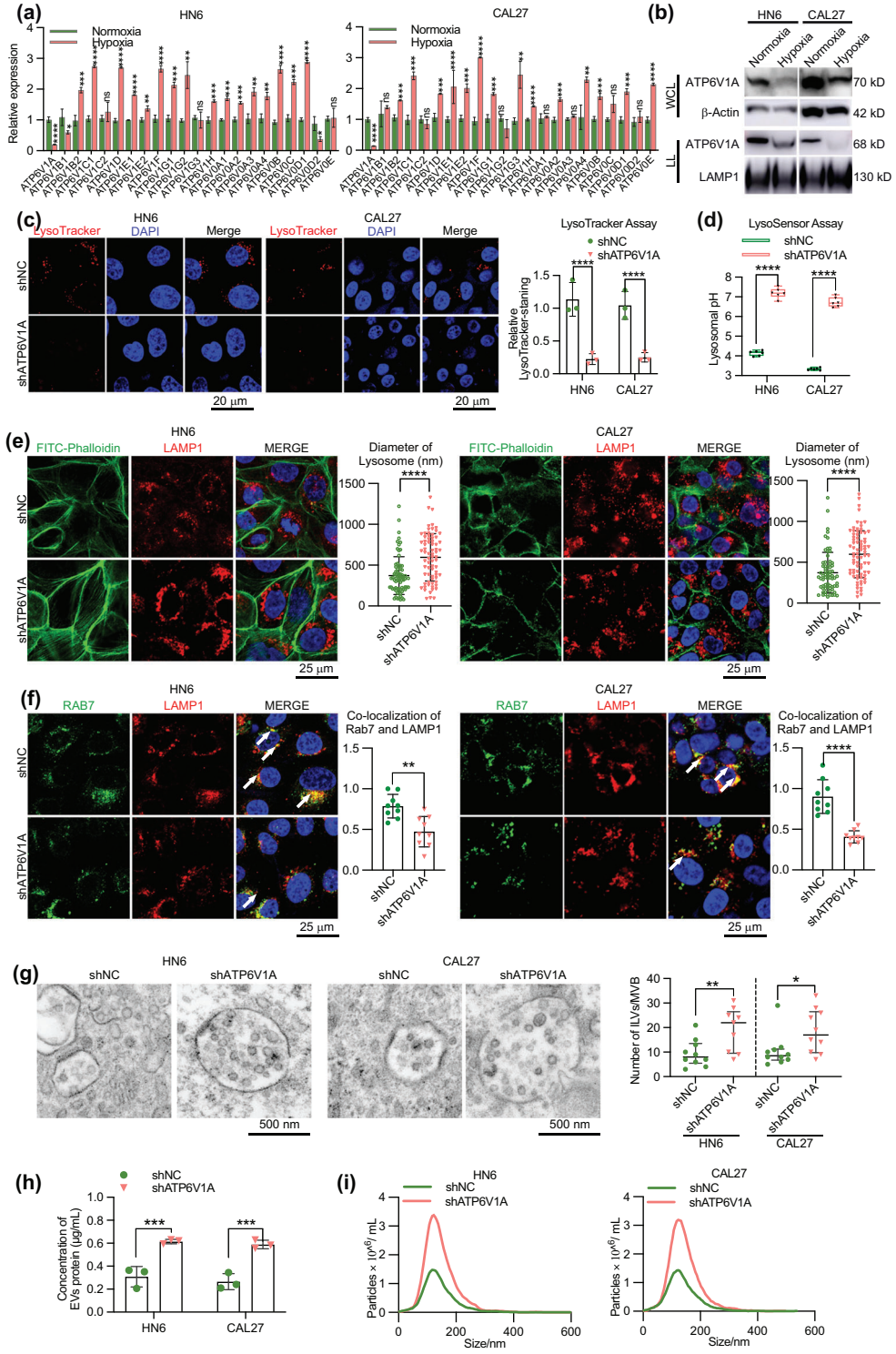

FIGURE 4 Hypoxia impairs lysosomal function by repressing the expression of ATP6V1A. (a) Real-time PCR was used to detect the effect of hypoxia on the expression of subunits of v-ATPase complex. (b) HN6 and CAL27 cells were exposed to normoxia or hypoxia for 48 h, and western blot was used to assess the protein level of ATP6V1A in whole cell lysates (WCL) and lysosome lysates (LL). (c) shNC and shATP6V1A cells were stained with Lysotracker Red and Lysotracker^{+} dots were quantified. Scale bar, 20 μm. (d) Lysosomal pH was determined in shNC and shATP6V1A cells. (e) Confocal microscopy analysis of the lysosome marker LAMP1 in shNC and shATP6V1A cells. Scale bar, 25 μm. The right graph shows the distribution of the lysosomal diameter ($n > 70$ per group). (f) Confocal co-localization analysis of lysosomal maker LAMP1 (red) and MVB marker Rab7 (green) in shNC and shATP6V1A cells. Scale bar, 25 μm. The ratio of co-localization of LAMP1 and Rab7 was quantified ($n > 10$ per group). (g) Electron microscopy images showing MVBs in shNC and shATP6V1A cells. Scale bar, 500 nm. Right graph: quantification of ILV number per MVB. Each dot represents the number of ILVs per MVB ($n > 10$ per group). (h) The EVs were collected from equal numbers of shNC/shATP6V1A cells and concentration of EV protein was measured using BCA assay. (i) The size and quantity of EVs from shNC/shATP6V1A cells were measured using NTA. EVs were collected from 20×10^6 cells for each group. Statistical analyses were performed using *t*-test. * *P*-value < 0.05. ** *P*-value < 0.01, *** *P*-value < 0.001, **** *P*-value < 0.0001. Data are presented as the mean ± S.D.

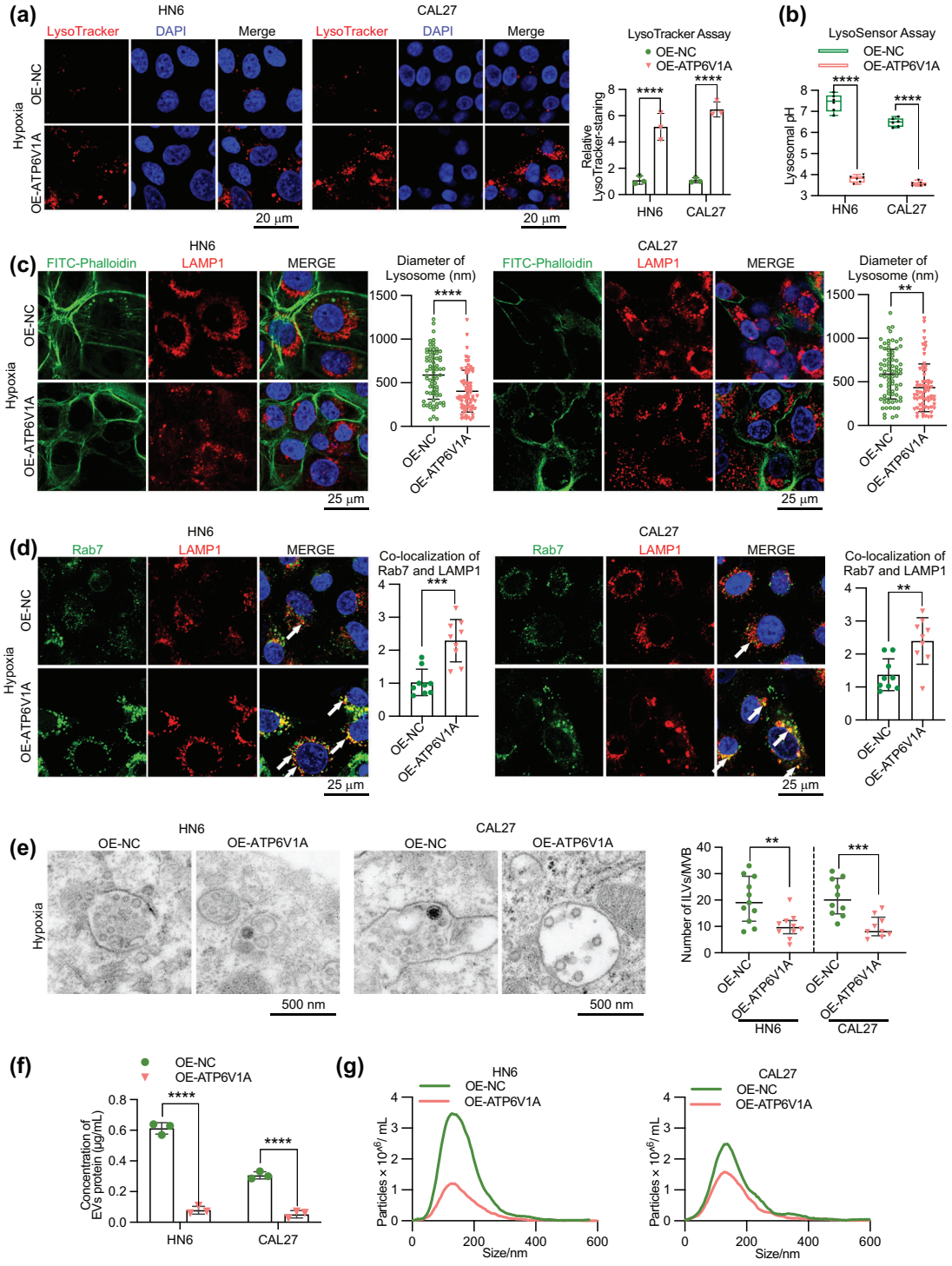

FIGURE 5 ATP6V1A is required for basal lysosomal function. (a) OE-NC and OE-ATP6V1A cells were cultured under hypoxia for 48 h, and stained with Lysotracker Red. Lysotracker^{+} dots were quantified. Scale bar, 20 μm. (b) Lysosomal pH was determined using Lysosensor™ Yellow/Blue DND-160 after cells were exposed to hypoxia for 48 h. (c) Confocal microscopy analysis of LAMP1 in OE-NC and OE-ATP6V1A cells to assess the size of lysosomes. Scale bar, 25 μm. The right graph shows the distribution of the lysosomal diameter ($n > 70$ per group). (d) Confocal co-localization analysis of LAMP1 and Rab7 in OE-NC and OE-ATP6V1A cells. Scale bar, 25 μm. The ratio of co-localization of LAMP1 and Rab7 was quantified ($n > 10$ per group). (e) Electron microscopy images showing MVBs in OE-NC and OE-ATP6V1A cells. Scale bar, 500 nm. Right graph: quantification of ILV number per MVB. Each dot represents the number of ILVs per MVB ($n > 10$ per group). (f) The EVs were collected from equal numbers of OE-NC/OE-ATP6V1A cells and concentration of EV protein was measured using BCA assay. (g) The size and quantity of EVs from OE-NC/ OE-ATP6V1A cells were measured using NTA. EVs were collected from 20×10^6 cells for each group. Statistical analyses were performed using *t*-test. ** *P*-value < 0.01, *** *P*-value < 0.001, **** *P*-value < 0.0001. Data are presented as the mean ± S.D.

the results above illustrate that the reactivation of ATP6V1A could rescue the hypoxia-induced phenotypes of the lysosomes and recover the lysosomal function of MVB degradation in the endolysosomal system.

Taken together, these results allowed us to conclude that hypoxia destroys the functions of lysosomes by reducing the expression of ATP6V1A, a component of lysosomal v-ATPase. Moreover, re-expression of ATP6V1A under hypoxia could recover the lysosomes from malfunction and restore the level of EV release. Next, we sought to explore the reasons underlying ATP6V1A downregulation.

3.5 | HIF-1α negatively regulates the expression of ATP6V1A

According to the above data, hypoxia could decrease the expression of ATP6V1A at the mRNA level, and we speculated that the regulation of ATP6V1A expression by hypoxia occurred at the transcriptional level. Subsequently, we predicted the potential transcription factors that bind to the promoter of ATP6V1A with the PROMO database (http://alggen.lsi.upc.es/cgi-bin/promo_v3/promo/promoinit.cgi?dirDB=TF_8.3), and HIF-1α, the most important regulatory factor under hypoxic stress, was listed (Supplementary File 3). Then, this result was validated in the JASPR database (https://jaspar.genereg.net, Supplementary File 3). We therefore examined the feasibility of HIF-1α as the transcription factor of ATP6V1A. To this end, we first transfected HN6 and CAL27 cells with a HIF-1α-expressing plasmid, and found that after the HIF-1α was overexpressed (Figure S7a), the expression of ATP6V1A was repressed at both mRNA and protein levels (Figure 6a,b). In normoxia, HIF-1α is maintained at a low basal level as a result of continuous proteasomal degradation, which depends on the hydroxylation by the O_2-dependent prolyl hydroxylase domain (PHD) proteins and the subsequent ubiquitination by von Hippel-Lindau (VHL) proteins (de Heer et al., 2020). Then, the PHD inhibitor molidustat was used to obstruct the ubiquitination of HIF-1α, and the results showed that the expression of ATP6V1A was mildly decreased after HIF-1α accumulated (Figure 6c,d). Next, we sought to investigate the HIF-1α binding site on the ATP6V1A promoter. We retrieved the database of ChIP-seq information from the Cistrome Data Browser (http://cistrome.org/db/#/) and identified multiple potential candidate binding sites (Figure S7b). Then, a ChIP assay was performed to confirm the specific binding site, and the data indicated that HIF-1α was enriched on the ATP6V1A promoter fragment at base +1to +444 and +565 to +714 (Figure 6e). To further confirm these data, reverse-ChIP was subsequently carried out (Figure 6f), and the results suggested the binding of HIF-1α to the ATP6V1A promoter (Figure 6g). Furthermore, a luciferase reporter assay was employed under normoxia and revealed that HIF-1α overexpression significantly inhibited luciferase activity in HNSCC cells expressing the wild-type ATP6V1A reporter, while mutations in the HIF-1α binding seed region of the ATP6V1A reporter abrogated the repressive effect of HIF-1α (Figure 6h,i). Moreover, we analysed the correlation between HIF-1α and ATP6V1A expression in HNSCC samples using immunohistochemistry (IHC) whose results showed that HIF-1α expression was negatively correlated with ATP6V1A expression ($R = -0.4839$, $p < 0.0001$) (Figure 6j,k). Altogether, these results demonstrate that HIF-1α could be the transcription factor of ATP6V1A and inhibit ATP6V1A expression.

Furthermore, to investigate the potential clinical implications of HIF-1α and ATP6V1A expression, we analysed the correlations between HIF-1α/ATP6V1A expression levels and the clinicopathological parameters of HNSCC patients. The results showed that higher HIF-1α expression was significantly correlated with increased depth of invasion (DOI), advanced tumour stage and clinical stage (Table S6). However, the expression levels of ATP6V1A showed no obvious correlations with clinicopathological parameters of HNSCC patient through our study (Table S7).

3.6 | Accumulation of HIF-1α can impair lysosomes and increase EV release

Finally, we explored the influence of HIF-1α accumulation on lysosomal homeostasis of lysosomes and EV secretion in normoxia. A HIF-1α-overexpressing cell model was constructed using lentivirus, and the LysoTracker-positive density analysis revealed an imbalance of lysosomal acidification (Figure 7a). Accordingly, the LysoSensor assay showed an increased pH value in the lysosomes after the exogenous expression of HIF-1α in a normoxic environment (Figure 7b). Immunohistochemistry confirmed the enlarged average lysosomal compartments (Figure 7c), while less colocalization of LAMP1 and Rab7 indicated reduced fusion of MVBs and lysosomes after HIF-1α was upregulated (Figure 7d). Importantly, the formation of ILVs in MVBs was increased in HIF-1α-overexpressing cells compared to control cells (Figure 7e). Last, as expected, the increased expression of HIF-1α encouraged the release of EVs (Figure 7f,g). Moreover, treatment with molidustat also promoted EV secretion (Figure S8). Collectively, HIF-1α could enhance EV release in HNSCC cells.

4 | DISCUSSION

Hypoxia is an essential hallmark of several serious diseases, including cancer. A decline in the tumour tissue oxygen level induces a hypoxic response in cells striving to adapt to the changed conditions, in which EVs serve as a significant mediator regulating

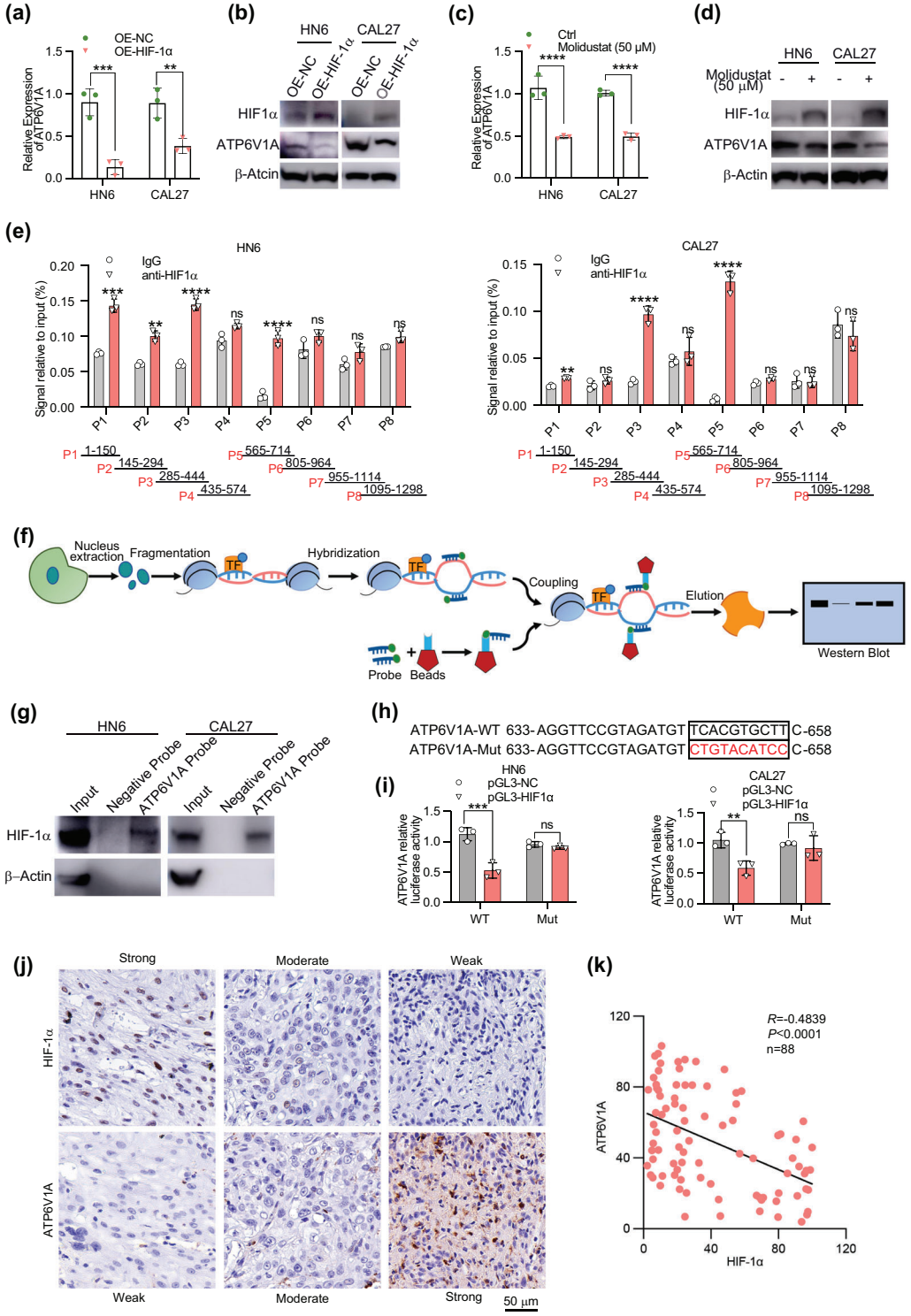

FIGURE 6 HIF-1α negatively regulated the expression of ATP6V1A. (a) Real-time PCR was performed to assess the expression of ATP6V1A after cells were transfected with HIF-1α for 48 h. (b) After cells were transfected with HIF-1α for 48 h, western blot was performed to detect the protein level of HIF-1α and ATP6V1A, using β-Actin as loading control. (c) HN6 and CAL27 cells were treated with molidustat (50 mM) for 48 h, and mRNA level of ATP6V1A was examined. (d) Western blot analysis of HIF-1α and ATP6V1A after 48-h treatment of molidustat (50 mM). (e) Cells were cultured under hypoxia for 48 h and collected, then ChIP-qPCR assay was performed to detect the binding of HIF-1α on the promoter region of ATP6V1A. (f) The schematic diagram of reverse-ChIP assay. (g) After HN6 and CAL27 cells were exposed to hypoxia for 48 h, nucleus extraction was collected and reverse-ChIP assay was performed to assess the binding of HIF-1α on the promoter region of ATP6V1A. (h) Construction of the wild-type/mutant ATP6V1A reporter. (i) Transcriptional activity was detected using dual-luciferase reporter assays in HN6 and CAL27 cells transfected with HIF-1α and luciferase reporters. (j) IHC analysis of HIF-1α and ATP6V1A expression levels in 88 HNSCC tissues. Image of weak, moderate and strong HIF-1α and ATP6V1A staining are shown. (**k**) The correlation of HIF-1α and ATP6V1A expression was analysed ($R = -0.4839$). Statistical analyses were performed using *t*-test. ns, no significance, ** *P*-value < 0.01, *** *P*-value < 0.001, **** *P*-value < 0.0001. Data are presented as the mean ± S.D.

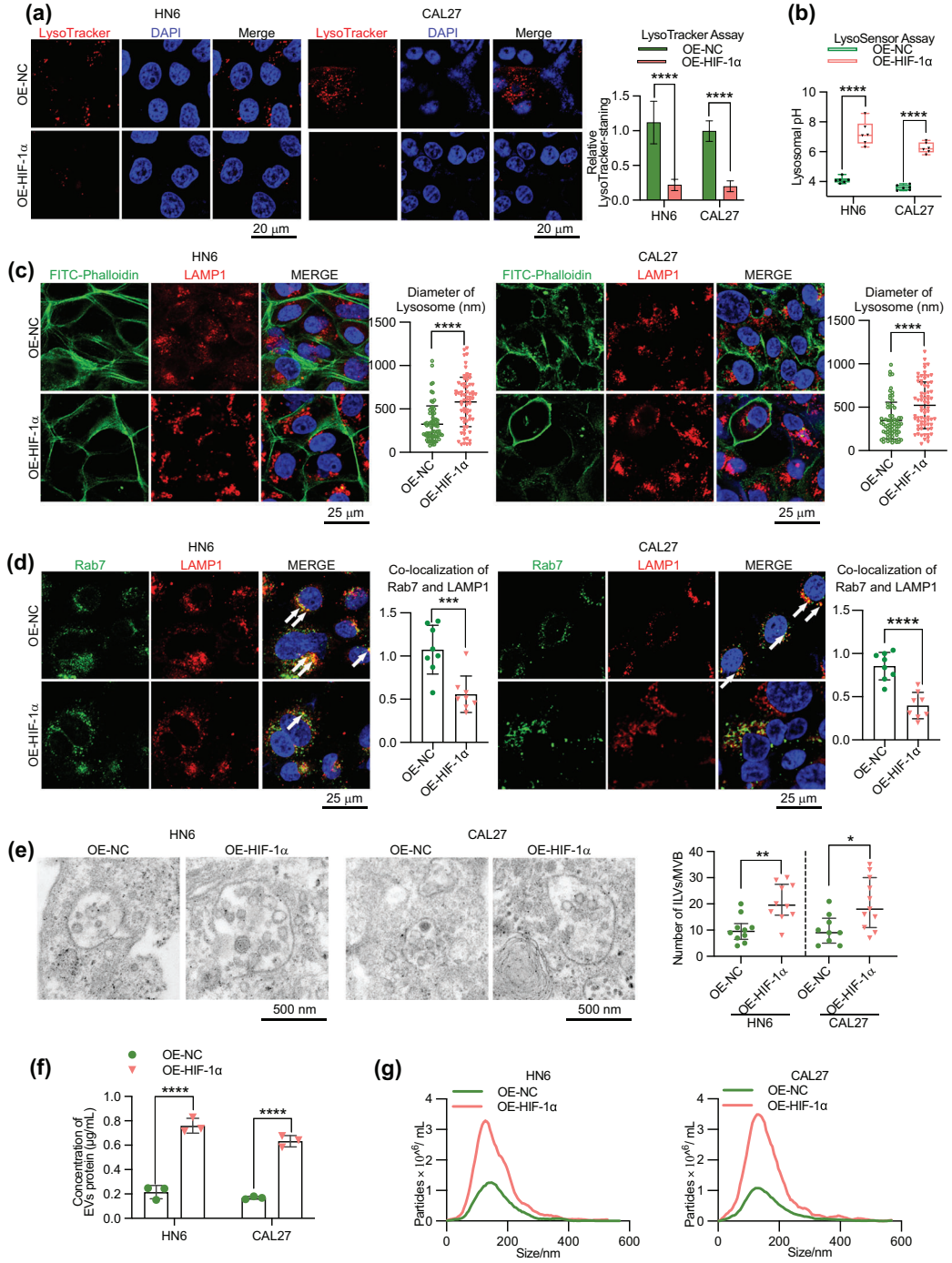

FIGURE 7 Accumulation of HIF-1α can impair lysosomes and promote EV secretion. (a) OE-NC and OE-HIF-1α cells were stained with Lysotracker Red and Lysotracker$^+$ dots were quantified. Scale bar, 20 μm. (b) Lysosomal pH of OE-NC and OE-HIF-1α cells was determined by Lysosensor assay. (c) Confocal microscopy analysis of LAMP1 in OE-NC and OE- HIF-1α cells to assess the size of lysosomes. Scale bar, 25 μm. The right graph shows the distribution of the lysosomal diameter ($n > 70$ per group). (d) Confocal co-localization analysis of LAMP1 and Rab7 in OE-NC and OE-HIF-1α cells. Scale bar, 25 μm. The ratio of co-localization of LAMP1 and Rab7 was quantified ($n > 10$ per group). (e) Electron microscopy images showing MVBs in OE-NC and OE-HIF-1α cells. Right graph: quantification of ILV number per MVB. Each dot represents the number of ILVs per MVB ($n > 10$ per group). Scale bar, 500 nm. (f) The EVs were collected from equal numbers of OE-NC/OE-HIF-1α cells and concentration of EV protein was measured using BCA assay. (g) The size and quantity of EVs from OE-NC/OE-HIF-1α cells were measured using NTA. EVs were collected from 20×10^6 cells for each group. Statistical analyses were performed using *t*-test. * *P*-value < 0.05. ** *P*-value < 0.01, *** *P*-value < 0.001, **** *P*-value < 0.0001. Data are presented as the mean ± S.D.

complex intercellular communication (Xi et al., 2021). Recent research shows that hypoxic tumours are at elevated risk for local failure and distant metastasis, which indicates a worse prognosis (Jing et al., 2019). Interestingly, analysis of the data from TCGA database demonstrated that HNSCC was one of the most hypoxic tumour among 19 tumour types (Bhandari et al., 2019). We performed a Kaplan-Meier analysis of HNSCC data from TCGA database and results showed higher hypoxic score was correlated with reduced overall survival (Figure S9).

A growing number of studies have clarified that tumour cells secrete more EVs under hypoxia to remodel the TME for survival (Kumar & Deep, 2020). In these studies, EV release was commonly measured by different methods, including total proteins, the quantity of EV-enriched markers or the number of particles (Hsu et al., 2017; King et al., 2012; Patton et al., 2020; Ren et al., 2019; Wang et al., 2014). In this study, total protein concentration measurements based on BCA and NTA were utilised to evaluate EV secretion and proved that there was an increase in the number of EVs in hypoxia compared to normoxia in HNSCC cells. In addition to the change in quantity, the contents of the EVs released by cells under hypoxic conditions also undergoes significant changes. Accumulating evidence has elucidated that tumour-derived hypoxic EVs can load aberrantly expressed biological information molecules that carry biological information, such as miRNAs, lncRNAs, proteins and other signalling factors, to transfer to recipient cells and facilitate tumour progression (Aga et al., 2014; Chen et al., 2018; Liang et al., 2020; Llorente et al., 2013; Melo et al., 2014; Shan et al., 2018; Umezu et al., 2014). The above researches suggest that the content change of hypoxic EVs carries considerable weight in remodelling the tumour microenvironment. Nevertheless, an in-depth study is needed in the future.

The term 'extracellular vesicle' actually encompasses a number of biogenetically distinct membranous structures, and some researchers speculate that since they are generated at different sites, EVs from different sources of biogenesis will likely contain different sets of specific cargoes and thus probably different functions (Bister et al., 2020). One typical obstacle in the field of EV research is distinguishing EVs of different origins, as these populations show overlap in terms of composition and size (Thery et al., 2018). However, some attempts have been made to identify specific markers defining the different subtypes of EVs. Kowal et al demonstrated that EVs bearing only CD9 or CD81 but not CD63 probably did not form in the endosomal system, whereas those bearing CD63 together with one or the two other tetraspanins may correspond to endosome-derived exosomes (Kowal et al., 2016). Recently, Mathieu et al further identified several specific markers to distinguish EVs of different origins (Mathieu et al., 2021). Based on the results of these studies, we determined that the hypoxia enhances the secretion of EVs of endosomal origin instead of those from the plasma membrane. Moreover, the overexpression of most components of the ESCRT complex in hypoxia confirmed by mRNA array indicated a more active status of the endosomal system. In addition to the ESCRT machinery, the MVB pathway may also be regulated by members of the Rab GTPase family, since Rab GTPases are localized on the surface of distinct intracellular membranes and regulate their vesicular transport through the recruitment of specific effector proteins (Jean & Kiger, 2012; Stenmark, 2009). Rab27a is one of the most well-studied Rab GTPases, which is required for MVB docking and fusion with the plasma membrane to release EVs. Currently, interfering with the expression of Rab27a has been a common method to inhibit EV secretion (Ostrowski et al., 2010; Poggio et al., 2019; Song et al., 2019). Given that we also investigated the impact of hypoxia on Rab27a, the data did not show a significant difference (Figure S10).

In solid tumours, the extracellular environment is harsh and imposes different types of stress on cells, such as hypoxia, nutrient deprivation and inflammation. After continuous exposure to hypoxia, the lysosomal functions of tumour cells undergo serious dysregulation (Ordway et al., 2021). An increasing number of studies have provided direct or indirect evidence suggesting that impairment of lysosomes under hypoxia is mainly characterized by aberrant position (Walton et al., 2018) and increased pH. In this study, LAMP1, the structural protein of lysosomes, was used to assess the presence of intracellular lysosomes. Immunoblotting and fluorescence assay both revealed no clear impact on the biogenesis of lysosomes in hypoxia, which was consistent with previous study (Lucien et al., 2017). This disequilibrium of the acidic lysosomal environment was the main form of impairment under hypoxia in HNSCC cells, which contributed to severe lysosomal dysfunction.

In the endosomal transport network, Rab5-Rab7 conversion regulates the transition from early to late endosomes (Poteryaev et al., 2010). In essence, vacuolar regions detach and bud inward to form ILVs of MVBs, also called the maturation of late endosomes, and Rab7 is mainly located in late endosomes in eukaryotic cells (Galvez et al., 2012). These ILVs can represent pre-secreted EVs that may be expelled into the extracellular space upon fusion of MVBs with the plasm membrane. However, according to the current research, the main fate of MVBs is fusion with lysosomes, leading to the degradation of their contents (van Niel et al., 2022). Our data clearly showed that lysosomal malfunction caused by hypoxia or ATP6V1A knockdown could interrupt this fusion and facilitate the accumulation of ILVs in MVBs, and ultimately contributing to the release of EVs.

Lysosomal acidification is regulated by v-ATPase, a multisubunit protein complex composed of the cytosolic V1 sector and the lysosomal membrane-anchored V0 sector (Bagh et al., 2017). We assessed the expression of all subunits that formed the complex and confirmed that ATP6V1A is the most affected subunit. Our further experiments suggest that ATP6V1A plays an important role in maintaining the homeostasis of lysosomes. In addition, several studies have revealed the abnormal expression of ATP6V1A in tumours and found that a high expression level of the ATP6V1A gene suggests better prognosis (Fernandez-Mosquera et al., 2019; Latifkar et al., 2019; Latifkar et al., 2022; Li, Li et al., 2020; Wang et al., 2017). Our study may provide new insight into the role of ATP6V1A in tumour progression.

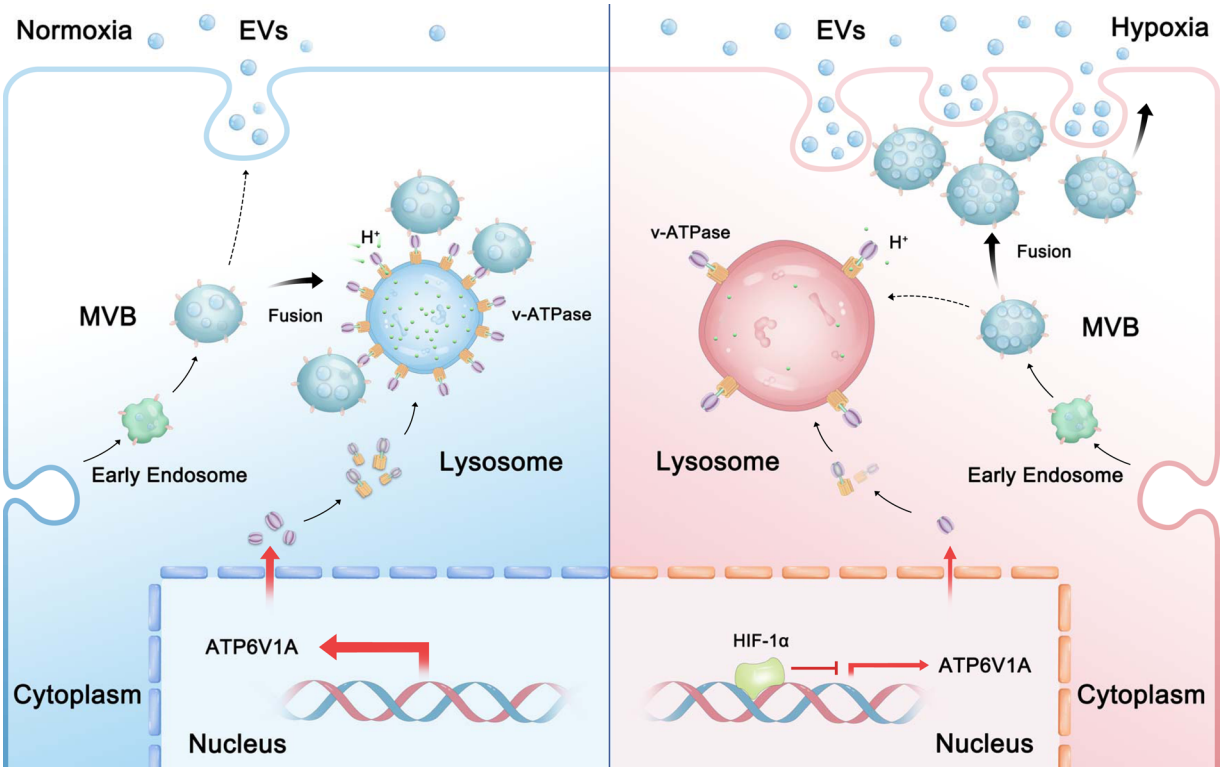

FIGURE 8 A schematic diagram of proposed mechanism.

Data from public databases showed the potential binding of HIF-1α to the ATP6V1A promoter. Subsequently, ChIP and reverse-ChIP confirmed that HIF-1α can target the promoter region of ATP6V1A. As the most important regulator under hypoxia, HIF-1α is reported to regulate a large number of genes and influence tumour development in many different ways (Albadari et al., 2019; Balamurugan, 2016; Choudhry & Harris, 2018; Li, Mao et al., 2020; Miles et al., 2017; Semenza, 2013; Xiaofei et al., 2018). However, as a transcription factor, few studies have reported the direct negative regulatory role of HIF-1α. Through a literature review, we found that most verified transcription factors able to act as transcriptional repressor, such like YY1, ID2 and δEF1, would bind to a specific palindromic sequence motif (CANNTG) known as the E-box of the gene promoter (Chen et al., 2012; Okazaki & Sandell, 2004; Ye & Young, 1997). Coincidentally, in our study, using a luciferase reporter assay we proved that HIF-1α could bind to E-box motif of ATP6V1A promoter and downregulate its expression, and this effect was abrogated when the E-box sequence was mutated. In addition, our data verify that overexpression of HIF-1α and inhibition of HIF-1α ubiquitination can impair the function of lysosomes and promote EV secretion. Besides, the effect of increasing EV release by HIF-1α was reported in several studies (King et al., 2012; Muniz-Garcia et al., 2022). For instance, King et al reported that the increased expression of many plasma membrane receptors regulated by HIF-1α can lead to their self-activation, which consequently induces endocytosis and promotes EV release. We believe our results extend the understanding of the mechanism by which HIF-1α facilitates EV secretion.

To understand how cells modulate EV production under pathophysiological conditions has been a long-standing goal, since it is of significance to define the physiological relevance of cellular homeostasis and EV release, as well as to manipulate EVs as therapeutics. In this study, we elucidated that the accumulation of HIF-1α in HNSCC cells under hypoxia could repress the expression of ATP6V1A, an important component of lysosomal v-ATPase, thus disturbing the acidic balance in the lysosomes. Lysosomal dysfunction subsequently leads to reduced fusion with MVBs, finally increasing EV release (Figure 8). Our present study demonstrates a new regulatory mechanism of the balance between lysosomal homeostasis and EV secretion.

AUTHOR CONTRIBUTIONS

Xiaoning Wang: Conceptualization; Formal analysis; Funding acquisition; Investigation; Methodology; Project administration; Supervision; Validation; Visualization; Writing—original draft; Writing—review & editing. **Ruoyi Wu**: Formal analysis; Investigation; Methodology; Supervision; Validation; Visualization; Writing—review & editing. **Peisong Zhai**: Formal analysis; Investigation; Methodology; Supervision; Writing—review & editing. **Zheqi Liu**: Data curation; Investigation; Methodology. **Ronghui Xia**: Methodology; Supervision; Writing—review & editing. **Zhen Zhang**: Investigation; Methodology; Writing—review & editing. **Xing Qin**: Conceptualization; Supervision; Writing—review & editing. **Chuwen Li**: Methodology. **Wantao**

Chen: Conceptualization; Formal analysis; Funding acquisition; Investigation; Project administration; Supervision; Writing—review & editing. **Jiang Li**: Conceptualization; Formal analysis; Funding acquisition; Investigation; Project administration; Supervision; Validation; Writing—review & editing. **Jianjun Zhang**: Conceptualization; Data curation; Formal analysis; Funding acquisition; Investigation; Methodology; Project administration; Supervision; Validation; Writing—original draft; Writing—review & editing.

ACKNOWLEDGEMENTS

The authors acknowledge the assistance of their colleagues at Department of Oral Pathology and the Department of Oral and Maxillofacial-Head and Neck Oncology, Ninth People's Hospital, School of Medicine, Shanghai Jiao Tong University.

CONFILCT OF INTERESTS

The authors declare that they have no competing interests.

ORCID

Jianjun Zhang https://orcid.org/0000-0002-8329-2357

REFERENCES

Aga, M., Bentz, G. L., Raffa, S., Torrisi, M. R., Kondo, S., Wakisaka, N., Yoshizaki, T., Pagano, J. S., & Shackelford, J. (2014). Exosomal HIF1alpha supports invasive potential of nasopharyngeal carcinoma-associated LMP1-positive exosomes. *Oncogene*, *33*, 4613–4622.

Ahmad, F., & Leake, D. S. (2019). Lysosomal oxidation of LDL alters lysosomal pH, induces senescence, and increases secretion of pro-inflammatory cytokines in human macrophages. *Journal of Lipid Research*, *60*, 98–110.

Albadari, N., Deng, S., & Li, W. (2019). The transcriptional factors HIF-1 and HIF-2 and their novel inhibitors in cancer therapy. *Expert Opinion on Drug Discovery*, *14*, 667–682.

Amin, M. B., Greene, F. L., Edge, S. B., Compton, C. C., Gershenwald, J. E., Brookland, R. K., Meyer, L., Gress, D. M., Byrd, D. R., & Winchester, D. P. (2017). The eighth edition AJCC cancer staging manual: Continuing to build a bridge from a population-based to a more "personalized" approach to cancer staging. *CA Cancer Journal for Clinicians*, *67*, 93–99.

Bagh, M. B., Peng, S., Chandra, G., Zhang, Z., Singh, S. P., Pattabiraman, N., Liu, A., & Mukherjee, A. B. (2017). Misrouting of v-ATPase subunit V0a1 dysregulates lysosomal acidification in a neurodegenerative lysosomal storage disease model. *Nature Communications*, *8*, 14612.

Baietti, M. F., Zhang, Z., Mortier, E., Melchior, A., Degeest, G., Geeraerts, A., Ivarsson, Y., Depoortere, F., Coomans, C., Vermeiren, E., Zimmermann, P., & David, G. (2012). Syndecan-syntenin-ALIX regulates the biogenesis of exosomes. *Nature Cell Biology*, *14*, 677–685.

Balamurugan, K. (2016). HIF-1 at the crossroads of hypoxia, inflammation, and cancer. *International Journal of Cancer*, *138*, 1058–1066.

Bhandari, V., Hoey, C., Liu, L. Y., Lalonde, E., Ray, J., Livingstone, J., Lesurf, R., Shiah, Y. J., Vujcic, T., Huang, X., Espiritu, S. M. G., Heisler, L. E., Yousif, F., Huang, V., Yamaguchi, T. N., Yao, C. Q., Sabelnykova, V. Y., Fraser, M., Chua, M. L. K., … Bristow, R. G. (2019). Molecular landmarks of tumour hypoxia across cancer types. *Nature Genetics*, *51*, 308–318.

Bister, N., Pistono, C., Huremagic, B., Jolkkonen, J., Giugno, R., & Malm, T. (2020). Hypoxia and extracellular vesicles: A review on methods, vesicular cargo and functions. *Journal of Extracellular Vesicles*, *10*, e12002.

Bjornetro, T., Redalen, K. R., Meltzer, S., Thusyanthan, N. S., Samiappan, R., Jegerschold, C., Handeland, K. R., & Ree, A. H. (2019). An experimental strategy unveiling exosomal microRNAs 486-5p, 181a-5p and 30d-5p from hypoxic tumour cells as circulating indicators of high-risk rectal cancer. *Journal of Extracellular Vesicles*, *8*, 1567219.

Breiden, B., & Sandhoff, K. (2019). Lysosomal Glycosphingolipid Storage Diseases. *Annual Review of Biochemistry*, *88*, 461–485.

Chen, X., Zhou, J., Li, X., Wang, X., Lin, Y., & Wang, X. (2018). Exosomes derived from hypoxic epithelial ovarian cancer cells deliver microRNAs to macrophages and elicit a tumour-promoted phenotype. *Cancer Letter*, *435*, 80–91.

Chen, X. S., Zhang, Y. H., Cai, Q. Y., & Yao, Z. X. (2012). ID2: A negative transcription factor regulating oligodendroglia differentiation. *Journal of Neuroscience Research*, *90*, 925–932.

Choudhry, H., & Harris, A. L. (2018). Advances in hypoxia-inducible factor biology. *Cell Metabolism*, *27*, 281–298.

Damaghi, M., Tafreshi, N. K., Lloyd, M. C., Sprung, R., Estrella, V., Wojtkowiak, J. W., Morse, D. L., Koomen, J. M., Bui, M. M., Gatenby, R. A., & Gillies, R. J. (2015). Chronic acidosis in the tumour microenvironment selects for overexpression of LAMP2 in the plasma membrane. *Nature Communications*, *6*, 8752.

de Heer, E. C., Jalving, M., & Harris, A. L. (2020). HIFs, angiogenesis, and metabolism: Elusive enemies in breast cancer. *Journalof Clinical Investigation*, *130*, 5074–5087.

DePedro, H. M., & Urayama, P. (2009). Using LysoSensor yellow/blue DND-160 to sense acidic pH under high hydrostatic pressures. *Analytical Biochemistry*, *384*, 359–361.

Dorayappan, K. D. P., Wanner, R., Wallbillich, J. J., Saini, U., Zingarelli, R., Suarez, A. A., Cohn, D. E., & Selvendiran, K. (2018). Hypoxia-induced exosomes contribute to a more aggressive and chemoresistant ovarian cancer phenotype: A novel mechanism linking STAT3/Rab proteins. *Oncogene*, *37*, 3806–3821.

Fernandez-Mosquera, L., Yambire, K. F., Couto, R., Pereyra, L., Pabis, K., Ponsford, A. H., Diogo, C. V., Stagi, M., Milosevic, I., & Raimundo, N. (2019). Mitochondrial respiratory chain deficiency inhibits lysosomal hydrolysis. *Autophagy*, *15*, 1572–1591.

Forgac, M. (2007). Vacuolar ATPases: Rotary proton pumps in physiology and pathophysiology. *Nature Reviews Molecular Cell Biology*, *8*, 917–929.

Galvez, T., Gilleron, J., Zerial, M., & O'Sullivan, G. A. (2012). SnapShot: Mammalian Rab proteins in endocytic trafficking. *Cell*, *151*, 234–234. e232.

Glunde, K., Guggino, S. E., Solaiyappan, M., Pathak, A. P., Ichikawa, Y., & Bhujwalla, Z. M. (2003). Extracellular acidification alters lysosomal trafficking in human breast cancer cells. *Neoplasia*, *5*, 533–545.

Guo, X., Qiu, W., Liu, Q., Qian, M., Wang, S., Zhang, Z., Gao, X., Chen, Z., Xue, H., & Li, G. (2018). Immunosuppressive effects of hypoxia-induced glioma exosomes through myeloid-derived suppressor cells via the miR-10a/Rora and miR-21/Pten Pathways. *Oncogene*, *37*, 4239–4259.

Hanahan, D., & Weinberg, R. A. (2011). Hallmarks of cancer: The next generation. *Cell*, *144*, 646–674.

Heaton, R. A., Heales, S., Rahman, K., Sexton, D. W., & Hargreaves, I. (2020). The effect of cellular coenzyme Q10 deficiency on lysosomal acidification. *Journal of Clinical Medicine*, 9.

Henne, W. M., Buchkovich, N. J., & Emr, S. D. (2011). The ESCRT pathway. *Developmental Cell*, *21*, 77–91.

Hong, J., Wuest, T. R., Min, Y., & Lin, P. C. (2019). Oxygen tension regulates lysosomal activation and receptor tyrosine kinase degradation. *Cancers (Basel)*, 11.

Hou, P. P., & Chen, H. Z. (2021). Extracellular vesicles in the tumour immune microenvironment. *Cancer Letters*, *516*, 48–56.

Hsu, Y. L., Hung, J. Y., Chang, W. A., Lin, Y. S., Pan, Y. C., Tsai, P. H., Wu, C. Y., & Kuo, P. L. (2017). Hypoxic lung cancer-secreted exosomal miR-23a increased angiogenesis and vascular permeability by targeting prolyl hydroxylase and tight junction protein ZO-1. *Oncogene*, *36*, 4929–4942.

Jean, S., & Kiger, A. A. (2012). Coordination between RAB GTPase and phosphoinositide regulation and functions. *Nature Reviews Molecular Cell Biology*, *13*, 463–470.

Jing, X., Yang, F., Shao, C., Wei, K., Xie, M., Shen, H., & Shu, Y. (2019). Role of hypoxia in cancer therapy by regulating the tumour microenvironment. *Molecular Cancer*, *18*, 157.

King, H. W., Michael, M. Z., & Gleadle, J. M. (2012). Hypoxic enhancement of exosome release by breast cancer cells. *BMC Cancer*, *12*, 421.

Kowal, J., Arras, G., Colombo, M., Jouve, M., Morath, J. P., Primdal-Bengtson, B., Dingli, F., Loew, D., Tkach, M., & Thery, C. (2016). Proteomic comparison defines novel markers to characterize heterogeneous populations of extracellular vesicle subtypes. *Proceedings of National Academy of Sciences U S A*, *113*, E968–E977.

Kumar, A., & Deep, G. (2020). Hypoxia in tumour microenvironment regulates exosome biogenesis: Molecular mechanisms and translational opportunities. *Cancer Letters*, *479*, 23–30.

Latifkar, A., Ling, L., Hingorani, A., Johansen, E., Clement, A., Zhang, X., Hartman, J., Fischbach, C., Lin, H., Cerione, R. A., & Antonyak, M. A. (2019). Loss of sirtuin 1 alters the secretome of breast cancer cells by impairing lysosomal integrity. *Developmental Cell*, *49*, 393–408. e397.

Latifkar, A., Wang, F., Mullmann, J. J., Panizza, E., Fernandez, I. R., Ling, L., Miller, A. D., Fischbach, C., Weiss, R. S., Lin, H., Cerione, R. A., & Antonyak, M. A. (2022). IGF2BP2 promotes cancer progression by degrading the RNA transcript encoding a v-ATPase subunit. *Proceedings of National Academy of Sciences U S A*, *119*, e2200477119.

Li, L., Li, C., Wang, S., Wang, Z., Jiang, J., Wang, W., Li, X., Chen, J., Liu, K., Li, C., & Zhu, G. (2016). Exosomes derived from hypoxic oral squamous cell carcinoma cells deliver mir-21 to normoxic cells to elicit a prometastatic phenotype. *Cancer Research*, *76*, 1770–1780.

Li, T., Mao, C., Wang, X., Shi, Y., & Tao, Y. (2020). Epigenetic crosstalk between hypoxia and tumour driven by HIF regulation. *Journal of Experimental & Clinical Cancer Research*, *39*, 224.

Li, X., Li, H., Yang, C., Liu, L., Deng, S., & Li, M. (2020). Comprehensive analysis of ATP6V1s family members in renal clear cell carcinoma with prognostic values. *Frontiers in Oncology*, *10*, 567970.

Liang, Y., Song, X., Li, Y., Chen, B., Zhao, W., Wang, L., Zhang, H., Liu, Y., Han, D., Zhang, N., Ma, T., Wang, Y., Ye, F., Luo, D., Li, X., & Yang, Q. (2020). LncRNA BCRT1 promotes breast cancer progression by targeting miR-1303/PTBP3 axis. *Molecular Cancer*, *19*, 85.

Liu, B., Palmfeldt, J., Lin, L., Colaco, A., Clemmensen, K. K. B., Huang, J., Xu, F., Liu, X., Maeda, K., Luo, Y., & Jaattela, M. (2018). STAT3 associates with vacuolar H(+)-ATPase and regulates cytosolic and lysosomal pH. *Cell Research*, *28*, 996–1012.

Llorente, A., Skotland, T., Sylvanne, T., Kauhanen, D., Rog, T., Orlowski, A., Vattulainen, I., Ekroos, K., & Sandvig, K. (2013). Molecular lipidomics of exosomes released by PC-3 prostate cancer cells. *Biochimica Biophysica Acta*, *1831*, 1302–1309.

Lucien, F., Pelletier, P. P., Lavoie, R. R., Lacroix, J. M., Roy, S., Parent, J. L., Arsenault, D., Harper, K., & Dubois, C. M. (2017). Hypoxia-induced mobilization of NHE6 to the plasma membrane triggers endosome hyperacidification and chemoresistance. *Nature Communications*, *8*, 15884.

Mathieu, M., Nevo, N., Jouve, M., Valenzuela, J. I., Maurin, M., Verweij, F. J., Palmulli, R., Lankar, D., Dingli, F., Loew, D., Rubinstein, E., Boncompain, G., Perez, F., & Thery, C. (2021). Specificities of exosome versus small ectosome secretion revealed by live intracellular tracking of CD63 and CD9. *Nature Communications*, *12*, 4389.

Melo, S. A., Sugimoto, H., O'Connell, J. T., Kato, N., Villanueva, A., Vidal, A., Qiu, L., Vitkin, E., Perelman, L. T., Melo, C. A., Lucci, A., Ivan, C., Calin, G. A., & Kalluri, R. (2014). Cancer exosomes perform cell-independent microRNA biogenesis and promote tumourigenesis. *Cancer Cell*, *26*, 707–721.

Miles, A. L., Burr, S. P., Grice, G. L., & Nathan, J. A. (2019). The vacuolar-ATPase complex and assembly factors, TMEM199 and CCDC115, control HIF1alpha prolyl hydroxylation by regulating cellular iron levels. *Elife*, *6*, e22693.

Mounir, M., Lucchetta, M., Silva, T. C., Olsen, C., Bontempi, G., Chen, X., Noushmehr, H., Colaprico, A., & Papaleo, E. (2019). New functionalities in the TCGAbiolinks package for the study and integration of cancer data from GDC and GTEx. *PLoS Computational Biology*, *15*, e1006701.

Muniz-Garcia, A., Romero, M., Falcomicronn-Perez, J. M., Murray, P., Zorzano, A., & Mora, S. (2022). Hypoxia-induced HIF1alpha activation regulates small extracellular vesicle release in human embryonic kidney cells. *Science Report*, *12*, 1443.

Nakashima, A., Cheng, S. B., Ikawa, M., Yoshimori, T., Huber, W. J., Menon, R., Huang, Z., Fierce, J., Padbury, J. F., Sadovsky, Y., Saito, S., & Sharma, S. (2020). Evidence for lysosomal biogenesis proteome defect and impaired autophagy in preeclampsia. *Autophagy*, *16*, 1771–1785.

Okazaki, K., & Sandell, L. J. (2004). Extracellular matrix gene regulation. *Clinical Orthopaedics and Related Research*, S123–S128.

Oot, R. A., Couoh-Cardel, S., Sharma, S., Stam, N. J., & Wilkens, S. (2017). Breaking up and making up: The secret life of the vacuolar H(+) -ATPase. *Protein Science*, *26*, 896–909.

Ordway, B., Gillies, R. J., & Damaghi, M. (2021). Extracellular acidification induces lysosomal dysregulation. *Cells*, 10.

Ostrowski, M., Carmo, N. B., Krumeich, S., Fanget, I., Raposo, G., Savina, A., Moita, C. F., Schauer, K., Hume, A. N., Freitas, R. P., Goud, B., Benaroch, P., Hacohen, N., Fukuda, M., Desnos, C., Seabra, M. C., Darchen, F., Amigorena, S., Moita, L. F., …Thery, C. (2010). Rab27a and Rab27b control different steps of the exosome secretion pathway. *Nature Cell Biology*, *12*, 19–30. sup pp 11–13.

Patton, M. C., Zubair, H., Khan, M. A., Singh, S., & Singh, A. P. (2020). Hypoxia alters the release and size distribution of extracellular vesicles in pancreatic cancer cells to support their adaptive survival. *Journal of Cellular Biochemistry*, *121*, 828–839.

Poggio, M., Hu, T., Pai, C. C., Chu, B., Belair, C. D., Chang, A., Montabana, E., Lang, U. E., Fu, Q., Fong, L., & Blelloch, R. (2019). Suppression of exosomal PD-L1 induces systemic anti-tumour immunity and memory. *Cell*, *177*, 414–427. e413.

Poteryaev, D., Datta, S., Ackema, K., Zerial, M., & Spang, A. (2010). Identification of the switch in early-to-late endosome transition. *Cell*, *141*, 497–508.

Qin, X., Guo, H., Wang, X., Zhu, X., Yan, M., Wang, X., Xu, Q., Shi, J., Lu, E., Chen, W., & Zhang, J. (2019). Exosomal miR-196a derived from cancer-associated fibroblasts confers cisplatin resistance in head and neck cancer through targeting CDKN1B and ING5. *Genome Biology*, *20*, 12.

Ren, R., Sun, H., Ma, C., Liu, J., & Wang, H. (2019). Colon cancer cells secrete exosomes to promote self-proliferation by shortening mitosis duration and activation of STAT3 in a hypoxic environment. *Cell and Biosciences*, *9*, 62.

Rong, L., Li, R., Li, S., & Luo, R. (2016). Immunosuppression of breast cancer cells mediated by transforming growth factor-beta in exosomes from cancer cells. *Oncology Letters*, *11*, 500–504.

Saftig, P., & Klumperman, J. (2009). Lysosome biogenesis and lysosomal membrane proteins: Trafficking meets function. *Nature Reviews Molecular Cell Biology*, *10*, 623–635.

Semenza, G. L (2013). HIF-1 mediates metabolic responses to intratumoural hypoxia and oncogenic mutations. *Journal of Clinical Investigation*, *123*, 3664–3671.

Shan, Y., You, B., Shi, S., Shi, W., Zhang, Z., Zhang, Q., Gu, M., Chen, J., Bao, L., Liu, D., & You, Y. (2018). Hypoxia-induced matrix metalloproteinase-13 expression in exosomes from nasopharyngeal carcinoma enhances metastases. *Cell Death & Disease*, *9*, 382.

Shao, C., Yang, F., Miao, S., Liu, W., Wang, C., Shu, Y., & Shen, H. (2018). Role of hypoxia-induced exosomes in tumour biology. *Molecualr Cancer*, *17*, 120.

Song, L., Tang, S., Han, X., Jiang, Z., Dong, L., Liu, C., Liang, X., Dong, J., Qiu, C., Wang, Y., & Du, Y. (2019). KIBRA controls exosome secretion via inhibiting the proteasomal degradation of Rab27a. *Nature Communication*, *10*, 1639.

Stenmark, H. (2009). Rab GTPases as coordinators of vesicle traffic. *Nature Reviews Molecular Cell Biology*, *10*, 513–525.

Thery, C., Witwer, K. W., Aikawa, E., Alcaraz, M. J., Anderson, J. D., Andriantsitohaina, R., Antoniou, A., Arab, T., Archer, F., Atkin-Smith, G. K., Ayre, D. C., Bach, J. M., Bachurski, D., Baharvand, H., Balaj, L., Baldacchino, S., Bauer, N. N., Baxter, A. A., Bebawy, M., … Zuba-Surma, E. K. (2018). Minimal information for studies of extracellular vesicles 2018 (MISEV2018): A position statement of the International Society for Extracellular Vesicles and update of the MISEV2014 guidelines. *Journal of Extracellular Vesicles*, *7*, 1535750.

Umezu, T., Tadokoro, H., Azuma, K., Yoshizawa, S., Ohyashiki, K., & Ohyashiki, J. H. (2014). Exosomal miR-135b shed from hypoxic multiple myeloma cells enhances angiogenesis by targeting factor-inhibiting HIF-1. *Blood*, *124*, 3748–3757.

van Niel, G., Carter, D. R. F., Clayton, A., Lambert, D. W., Raposo, G., & Vader, P. (2022). Challenges and directions in studying cell-cell communication by extracellular vesicles. *Nature Reviews Molecular Cell Biology*.

van Niel, G., D'Angelo, G., & Raposo, G. (2018). Shedding light on the cell biology of extracellular vesicles. *Nature Revies Molecular Cell Biology*, *19*, 213–228.

Walton, Z. E., Patel, C. H., Brooks, R. C., Yu, Y., Ibrahim-Hashim, A., Riddle, M., Porcu, A., Jiang, T., Ecker, B. L., Tameire, F., Koumenis, C., Weeraratna, A. T., Welsh, D. K., Gillies, R., Alwine, J. C., Zhang, L., Powell, J. D., & Dang, C. V. (2018). Acid Suspends the Circadian Clock in Hypoxia through Inhibition of mTOR. *Cell*, *174*, 72–87. e32.

Wang, P., Wang, L., Sha, J., Lou, G., Lu, N., Hang, B., Mao, J. H., & Zou, X. (2017). Expression and transcriptional regulation of human ATP6V1A gene in gastric cancers. *Science Report*, *7*, 3015.

Wang, T., Gilkes, D. M., Takano, N., Xiang, L., Luo, W., Bishop, C. J., Chaturvedi, P., Green, J. J., & Semenza, G. L. (2014). Hypoxia-inducible factors and RAB22A mediate formation of microvesicles that stimulate breast cancer invasion and metastasis. *Proceedings of National Academy of Science U S A*, *111*, E3234–E3242.

Weber, R. A., Yen, F. S., Nicholson, S. P. V., Alwaseem, H., Bayraktar, E. C., Alam, M., Timson, R. C., La, K., Abu-Remaileh, M., Molina, H., & Birsoy, K. (2020). Maintaining iron homeostasis is the key role of lysosomal acidity for cell proliferation. *Molecular Cell*, *77*, 645–655. e647.

Witwer, K. W., & Thery, C. (2019). Extracellular vesicles or exosomes? On primacy, precision, and popularity influencing a choice of nomenclature. *Journal of Extracellular Vesicles*, *8*, 1648167.

Xi, L., Peng, M., Liu, S., Liu, Y., Wan, X., Hou, Y., Qin, Y., Yang, L., Chen, S., Zeng, H., Teng, Y., Cui, X., & Liu, M. (2021). Hypoxia-stimulated ATM activation regulates autophagy-associated exosome release from cancer-associated fibroblasts to promote cancer cell invasion. *Journal of Extracellular Vesicles*, *10*, e12146.

Xiaofei, C., Yanqing, L., Dongkai, Z., Dong, C., Feng, Z., & Weilin, W. (2018). Identification of cathepsin B as a novel target of hypoxia-inducible factor-1-alpha in HepG2 cells. *Biochemical and Biophysical Research Communication*, *503*, 1057–1062.

Xie, Y., Liu, J., Kang, R., & Tang, D. (2020). Mitophagy receptors in tumour biology. *Frontiers Cell Developmental Biology*, *8*, 594203.

Yang, C., & Wang, X. (2021). Lysosome biogenesis: Regulation and functions. *Journal of Cellular Biology*, *00*, 220.

Ye, J., & Young, H. A. (1997). Negative regulation of cytokine gene transcription. *FASEB Journal*, *11*, 825–833.

SUPPORTING INFORMATION

Additional supporting information can be found online in the Supporting Information section at the end of this article.

How to cite this article: Wang, X., Wu, R., Zhai, P., Liu, Z., Xia, R., Zhang, Z., Qin, X., Li, C., Chen, W., Li, J., & Zhang, J. (2023). Hypoxia promotes EV secretion by impairing lysosomal homeostasis in HNSCC through negative regulation of ATP6V1A by HIF-1α. *Journal of Extracellular Vesicles*, *12,* e12310. https://doi.org/10.1002/jev2.12310